QUANTIFYING TYMPANIC MEMBRANE DYNAMICS IN OTITIS MEDIA USING LOW COHERENCE INTERFEROMETRY

BY

JUNGEUN WON

THESIS

Submitted in partial fulfillment of the requirements
for the degree of Master of Science in Bioengineering
in the Graduate College of the
University of Illinois at Urbana-Champaign, 2017

Urbana, Illinois

Advisor:

Professor Stephen A. Boppart

ABSTRACT

Examining middle ear dynamics and mobility of the tympanic membrane (TM) is essential when diagnosing otitis media (OM), or a middle ear infection. OM is a widespread infectious disease in childhood, characterized by the accumulation of middle ear fluid, known as middle ear effusion (MEE). Loss of TM mobility assessed by pneumatic otoscopy may help in determining the presence of a MEE, but its qualitative information has challenged its proper application. In order to provide more efficient and quantitative analysis of the TM dynamics, a pneumatic low-coherence interferometry (LCI) otoscope was developed with automated pressure generation.

The pneumatic LCI system developed during this research measures the TM displacement with an axial resolution of around 6.5 μm, and provides simultaneous pressure measurement in the ear canal with a temporal resolution of 1 msec. To facilitate the analysis, two quantitative metrics (compliance and amplitude ratio) were defined to compute the pneumatic mobility of the TM and the middle ear pressure (MEP). Followed by phantom studies and human subject testing, a total of 42 ear datasets from pneumatic LCI system and tympanometry were acquired from 30 pediatric outpatient subjects at Carle Foundation Hospital (Urbana, IL) to assess the clinical significance in relation to OM. As a result, the compliance and the amplitude ratio in the ears with OM were statistically lower than those in the normal group, showing the capability of the pneumatic LCI metrics to represent the TM mobility and characterize different middle ear conditions. The comparisons with current middle ear diagnostic devices, such as otoscopy and tympanometry, are discussed with the limitations of the study, and future directions for the research are presented in the conclusion. Overall, this thesis demonstrates the potential of non-invasive optical sensing and imaging methods to quantitatively describe the changes in middle ear dynamics experienced during OM.

ACKNOWLEDGEMENTS

I would like to thank my graduate advisor, Professor Stephen A. Boppart, for advice, guidance, and encouragement throughout research and professional development. I would like to thank all members of the Biophotonics Imaging Laboratory for helpful discussion and advice in understanding OCT principles, techniques, building OCT systems and handheld probe, conducting clinical research, and analyzing and dealing with the enormous datasets, specifically (in no particular order) Guillermo L. Monroy, Pin-Chieh Huang, Dr. Paritosh Pande, and Dr. Roshan Dsouza. I would like to thank Darold Spillman for administrative assistance and valuable advice, and Eric Chaney and Dr. Ronit Barkalifa for managements of IRB protocols.

I would like to thank our clinical collaborators at Carle Foundation Hospital, Dr. Malcolm Hill, Dr. Michael Novak, Dr. Ryan Porter, and nursing staffs from the department of Pediatrics at Windsor and the department of Otolaryngology at South Clinic, for subject recruitment, valuable data collection, and continuing interests in my research. I would also like to thank Carle Research Center, specifically Paula Bradley and Alexandra Almasov, for managing subject consents and assents, IRB protocols, and scheduling experiments.

Thanks to the staffs in the Bioengineering Department, and to my funding source, the National Institute of Health Bioengineering Research Partnership (R01 EB013723). Lastly, special thanks to my family for their support.

TABLE OF CONTENTS

1 INTRODUCTION

1.1 OVERVIEW

Otitis media (OM), more commonly known as a middle ear infection, is a highly prevalent pediatric disease worldwide, and its financial burden is continuously expected to increase due to chronic, recurring OM, and OM-associated complications [1]. Often accompanied with flu or allergies, an accumulation of middle ear fluid or middle ear effusions (MEEs) during OM may cause complications, such as tympanic membrane (TM) perforations and conductive hearing loss with language delay or behavioral problems [2]. Despite significant technical advances in biomedical imaging, traditional OM diagnostic methods based on otoscopy have remained the same since its development as early as in the mid 1300's [3]. Standard otoscopy visualizes the TM surface using a simple magnifying glass with an illumination source. When the added mass from MEEs in the middle ear cavity decreases mobility of the TM, dynamics of the TM can be examined by a pneumatic otoscope, a standard otoscope with an attachment of a pneumatic bulb. When performing pneumatic otoscopy, the ear canal is partially sealed by an ear speculum, allowing the physician to observe the movements of the TM in response to either negative or positive pressure, as the rubber pneumatic bulb is gently squeezed. Although pneumatic otoscopy is strongly recommended for physicians [4-6] to obtain a higher sensitivity in detecting MEEs [7], it is rarely used on a regular basis mainly due to a lack of quantitative information of the TM dynamics, the accuracy depending on a good seal of the ear canal, and the difficulty in subjectively interpreting the movements, limiting the appropriate analysis of middle ear dynamics and diagnostic accuracy [8, 9].

1.2 SCOPE OF RESEARCH

In this thesis, a quantitative method of measuring mobility of the TM and the middle ear dynamics is presented by combining low coherence interferometry (LCI) with pneumatic otoscopy, named as pneumatic LCI. An automated pressure generating module in the pneumatic LCI system creates controllable pressure transients, and its method will be described. Integrated with a handheld probe, this optically enhanced pneumatic otoscope provides not only high-resolution TM displacement traces, but also simultaneous pressure measurements, leading to the quantification of the TM mobility and middle ear pressure (MEP). The clinical significance of the system is assessed by phantom studies, *in vivo* measurements from a healthy adult volunteer, and *in vivo* measurements from pediatric outpatients at Carle Foundation Hospital (Urbana, IL). In addition, the measurements from the pneumatic LCI system are compared with standard tympanometry to validate defined pneumatic LCI metrics. The thesis includes a discussion of the limitations of the system as well as that of the study, suggesting future directions of the research. This study will potentially provide unique, valuable, and quantitative metrics that can help otologists and researchers understand the changes in middle ear dynamics experienced during OM.

1.3 OUTLINE

A literature review of OM, including pathophysiology, diagnosis and treatments, as well as a theoretical review of LCI and optical coherence tomography (OCT) are discussed in Chapter 2. LCI is the fundamental principle and technique used in OCT. Chapter 2 also reviews some recent optical middle ear imaging techniques, including but not limited to OCT. The specific aims of this research are included in Chapter 3. The detailed systematic, experimental, and analytical methods of the study are described in Chapter 4. The results of phantom and clinical studies are shown in

Chapter 5, followed by the discussion in Chapter 6. The discussion includes the effect of different middle ear dynamics on the changes in pneumatic mobility and MEP during OM, as well as the limitations of the study and the system. The conclusion with future directions are found in Chapter 7.

2 BACKGROUND

In this chapter, both biological and engineering background of the research are presented. Beginning with the anatomy of the middle ear and the tympanic membrane (TM), otitis media (OM) is described with its pathophysiology, treatment, and current methods of diagnosis. The fundamental theory of LCI and optical coherence tomography (OCT) are introduced, and previous and current research on optical middle ear imaging are summarized.

2.1 OTITIS MEDIA

Otitis media (OM) can be defined as any inflammation on the middle ear, where inflammation is referred to any biological immune response from damaging stimuli or injuries. The inflammatory response may occur with or without an infection, an invasion of microorganisms including viruses and/or bacteria. As a complex systemic inflammatory response, OM often presents with a variety of symptoms, such as low appetite, ear ache, fever, and headache [10]. A key characteristic of OM is the accumulation of fluid in a normally air-filled middle ear cavity, called a middle ear effusion (MEE). Statistically, approximately 90% of children will have at least one episode of OM before they enter school [11-13], and around 35-50% of them may revisit the clinic due to recurrent or persistent OM [2, 14]. Overall, there are around 30 million annual visits to physicians' offices due to OM [2], with national medical expenditures of around $ 4.1 billion [15]. In this section, the disease development of OM is illustrated with a review of the structures and functions of the middle ear and the TM. The different types of OM are explained based on the diagnostic guidelines and possible treatment options.

2.1.1 Middle Ear and Tympanic Membrane

The middle ear, shown in **Figure 1**, refers to the region between the TM and the oval window of the inner ear. The middle ear is subdivided into: the TM, middle ear cavity, ossicles (bones), and the Eustachian tube. The functions of the middle ear are to amplify and transmit sound waves from the outer ear to the inner ear. Initially, sound waves are collected and amplified through the ear canal. When sound waves are propagated through the TM, the acoustic energy of the sound waves is converted to mechanical energy, as the waves vibrate the TM. Due to the large surface membrane of the TM and coupled movements from ossicles of the middle ear, the energy is again amplified to a greater scale to facilitate hearing.

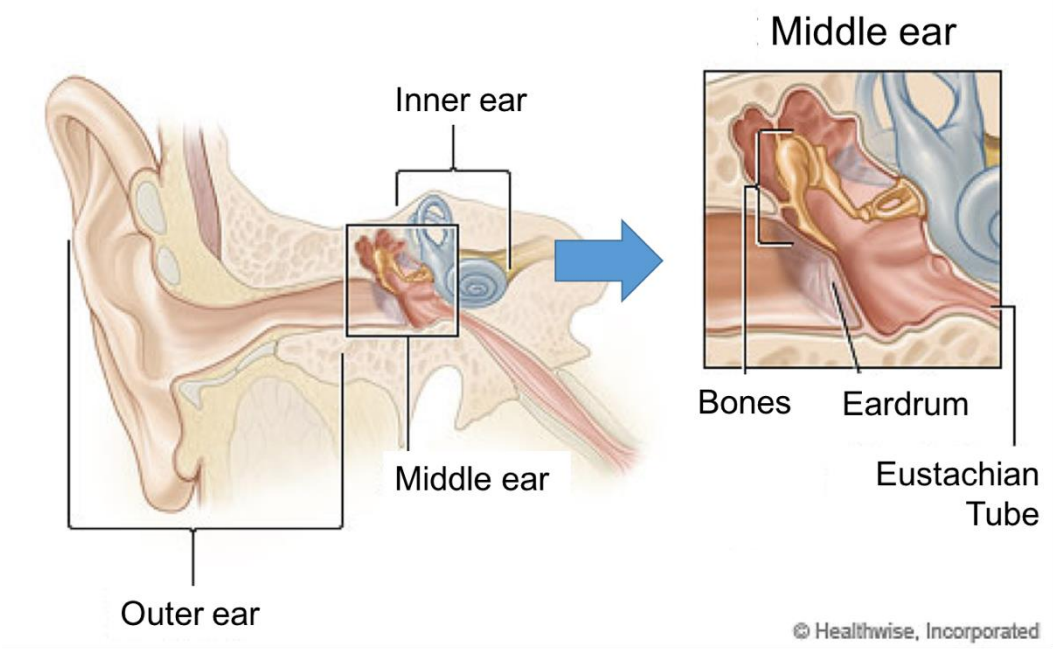

Figure 1. *Human ear diagram separated by the outer, middle, and inner ear. The zoomed in figure on the right shows middle ear components. Photo from [16].*

With an occurrence of OM, the process of converting the acoustic waves to the mechanical energy at the TM is largely affected. The accumulated MEE in the middle ear cavity reduces the TM mobility due to the added mass, viscosity, and pressure from the MEE, resulting in less

amplification of the acoustic energy and a distorted transduction process. As a result, the loss in TM mobility causes the acoustic dampening of sound, and disrupts the sound transmission to the inner ear. If a MEE does not resolve on its own and remains untreated, further complications, such as temporary hearing loss and chronic infections, may occur [2].

As a thin membrane that separates the middle ear from the outer ear, the TM may be the most vital and vulnerable structure during OM. The TM can be divided into two portions: the pars flaccida and the pars tensa, illustrated in **Figure 2**. The pars flaccida is in the upper region of the TM, and contains two layers, skin and mucosa. The pas tensa is in the lower, larger region of the TM, with an epithelial layer as the outermost layer, a fibrous layer in between, and a mucosal layer as the innermost layer. Although the pars flaccida has two layers, it is typically thicker than the pas tensa region due to the attachment to the ossicles. This variability in thickness and structures of the TM is important, as the TM mobility may be spatially-varying depending on the thickness. In addition, the thickness of the TM is often assessed by physicians, since inflammatory responses may thicken the TM.

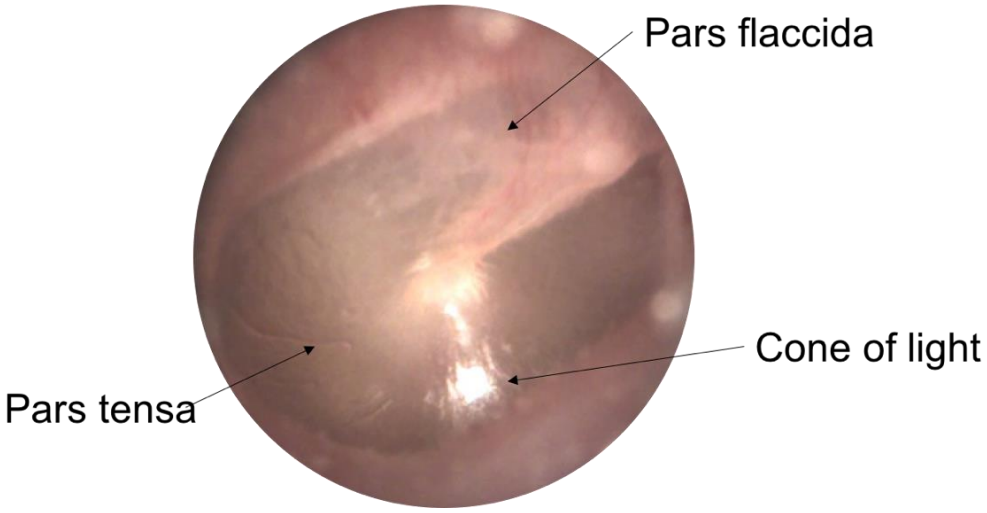

***Figure 2**. A wide-field view of the TM from the outer ear. Acquired from a healthy volunteer with a standard video otoscope from Wellch-Allyn.*

Another identifying structure of the TM is its overall cone-shaped structure oriented approximately 45 to 60 degrees to the ear canal to effectively amplify the mechanical energy converted from the sound waves [17-19]. Thus, when illuminated with light from a standard otoscope, a specific region, depending on the orientation, reflects the incident light more strongly than the other regions, called the "cone of light" (See **Figure 2**). Since the oriented angles and cone-shape of the TM vary as a MEE forms and the MEP increases in the middle ear cavity, the cone of light non-specifically and non-systematically changes during the time course of OM.

Anatomically, the TM can also be separated into four quadrants based on the handle of the malleus (one of ossicles) seen from the outer ear. With an imaginary line drawn along the handle of the malleus, and the second line perpendicular to the first line, the TM can be divided into: anterior inferior (AI), posterior inferior (PI), anterior superior (AS), and posterior superior (PS) segments, as shown in **Figure 3.** The cone of light is found in the AI region, and nerves and blood vessels pass through the superior portions of the TM.

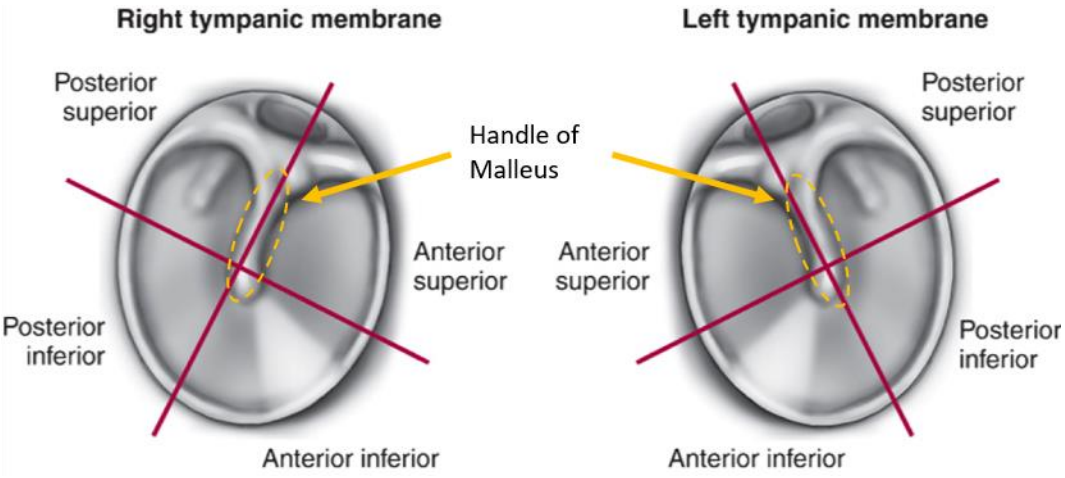

***Figure 3**. Quadrants of the right and left TM. Quadrants are determined based on the handle of malleus (one of ossicles). Photo from [20].*

As the TM is the only visibly accessible part of the middle ear *in vivo*, examining a full-field view of the TM is most helpful to determine the presence or absence of a MEE [10]. In addition, since the TM is typically translucent or semi-translucent, physicians may directly visualize MEEs by observing them through the TM. However, with inflammation, most TMs become partially or completely opaque, highly limiting the accuracy of visual diagnosis.

Besides the TM, the middle ear is also connected to the nasopharynx via the Eustachian tube, also shown in **Figure 1**. The Eustachian tube serves to equalize the pressure between the throat (ambient atmospheric pressure) and the middle ear. Equalization of the pressure is also important to hearing function as pressure differences between the middle ear and the outer ear restrict the motion of the TM and ossicles, causing conductive hearing loss. Another important function of the Eustachian tube is for fluid clearance from the middle ear cavity, as mucus is constantly generated in the middle ear cavity to keep the space moisturized, and to facilitate the transport and removal of macromolecules and any microorganisms [10, 21]. If the opening of the tube is restricted or blocked due to the swollen tissue from the inflammatory response, mucus may become trapped and start accumulating in the middle ear cavity. Therefore, it is worthwhile to mention that the initial process of OM is the dysfunction of the Eustachian tube.

2.1.2 Pathophysiology

The dysfunction of the Eustachian tube often occurs as a response from an infection from bacteria or viruses. In particular, the impairment of the Eustachian tube through allergies or an infection in the upper respiratory tract (URI) can trigger OM. *Streptococcus pneumoniae*, *Haemophilus influenza*, and *Moraxella catarrhalis* are the three most common types of bacteria causing OM in the United States [2], but these types may vary depending on the vaccinations, such as 13-valent

and 7-valent pneumococcal conjugate vaccine (PCV13 and PCV7, respectively), and antibiotics used in the country [10]. The common viruses responsible for OM include respiratory syncytial virus, adenovirus, and the influenza virus [22].

In general, bacteria or viruses entering the nasal cavity alter the Eustachian tube, creating a promoting environment for bacterial colonization, adhesion, and invasion of the microorganisms, as the proper drainage of mucus and the ventilation of the middle ear cavity becomes impaired [22]. As a result, the middle ear space becomes ideally suited for colonization by bacteria. In addition, the gas present in the middle ear is absorbed by the surrounding tissues due to the blocked Eustachian tube, creating a slight negative pressure. The TM may appear to be retracted during this stage. The negative pressure of the middle ear easily draws bacteria and/or viruses from the Eustachian tube to reach and spread the infectious microorganisms throughout the middle ear cavity. Once the bacteria are dispersed in the middle ear cavity, an inflammatory response occurs. Due to the inflammatory response, pus (thick, viscous material) is created and accumulates in the middle ear, now producing a more positive pressure with a bulging TM.

OM more frequently occurs in infants and children. OM is the second most common disease after URI, and is the leading cause for visits to medical clinics, for the prescription of antibiotics, and for surgical procedures during childhood [4, 10, 23]. One reason is that OM is often preceded by URIs and allergies, which children may be more vulnerable to. But more importantly, it is associated with an immature Eustachian tube. The Eustachian tube in children is more horizontal, shorter, and narrower, and the opening diameter is smaller than that of adults (See **Figure 4**). Therefore, the immature anatomy of the Eustachian tube and the developing immune system of infants and children readily lead to the dysfunction of the Eustachian tube, even without pathological infection [15, 24].

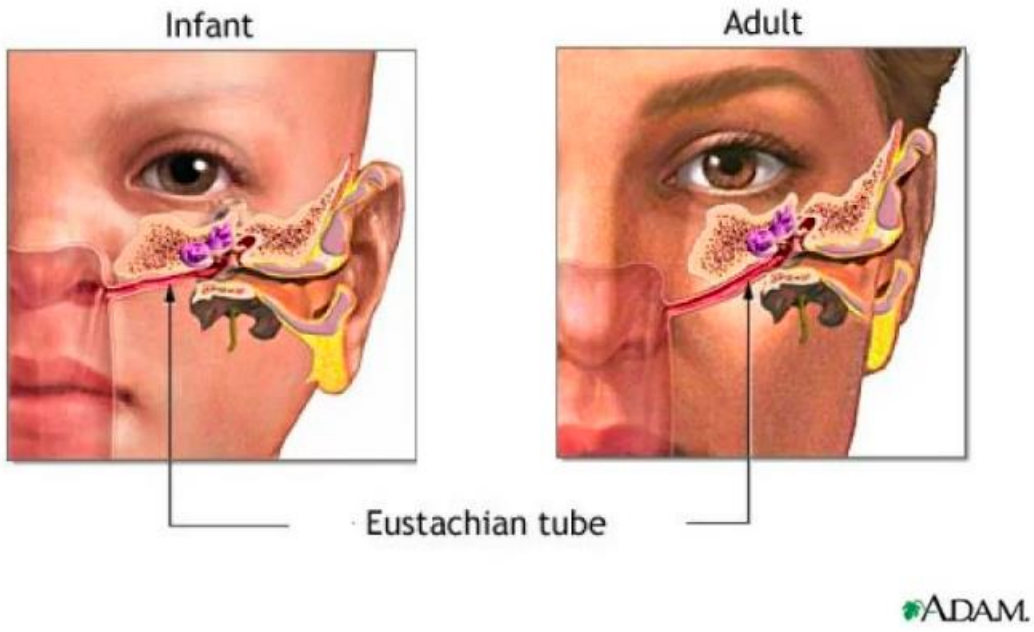

Figure 4. *Comparison of the Eustachian tube in an adult and a child. Photo from [25].*

2.1.3 Types of Otitis Media

This thesis mainly focuses on two types of OM: acute otitis media (AOM) and otitis media with effusion (OME). A patient would be diagnosed with one of these two types of OM if a MEE is found. AOM frequently occurs in younger children and infants, with the peak incidence between 6 to 12 months of age [11], and is characterized by an acute onset of an ear infection. The presence of an infection can be typically assessed by a bulging and opaque TM [4, 5]. Although several clinical manifestations exist based on the common symptoms related to bacterial or viral infections and the associated inflammation, these are generally not considered as good diagnostic criteria because of low sensitivity. **Table 1** lists common symptoms and visual manifestations with associated sensitivity and specificity for diagnosing OM [10].

Table 1. *Standard clinical manifestations used to diagnose otitis media. Data from [10].*

Source and Symptoms	Sensitivity (%)	Specificity (%)
Ear pain	54	82
Ear rubbing	42	87
Fever	40	48
Cough	47	45
Rhinitis	75	43
Excessive crying	55	69
Poor appetite	36	66
Vomiting	11	89
Sore throat	13	74
Headache	9	76

On the other hand, OME presents with the accumulation of a MEE without direct inflammation of the middle ear. In other words, OME is characterized by the presence of a MEE in the absence of signs or symptoms of an infection. Due to an absence of an infection, OME is often diagnosed by visualizing a semi-translucent TM with the presence of a MEE behind a retracted TM [6]. OME does not usually present with an ear ache or fever, but often with hearing problems. Nonetheless, a recent study showed that OME patients can also have an ear ache from the fullness of the ear, and present with fever if another infectious disease, such as a URI, accompanies the OME [10].

2.1.4 Treatment and Complications

The fundamental difference between OME and AOM is that OME does not present with a directly associated bacterial or viral infection, although bacteria or a virus can cause OME [2]. It is known that OME can occur during the healing process of AOM, or OME can follow AOM, but there is an emerging hypothesis that OME may also precede AOM [10]. Discriminating those two types is

highly challenging, but essential in diagnosing OM, since the initial treatment of AOM is to prescribe antibiotics, while that of OME can be watchful waiting [4, 6].

When determining treatment options, physicians first assess possible risks of complications based on age, stage and type of the OM, and the presence of other ear problems (i.e. cochlea implant), and focus on relieving ear ache. As OM can often resolve without medical treatments, there are several home treatments recommended by physicians in the early stages of OM. These include pain relievers for an ear ache, applying heat to the ear, and eardrops [2, 6]. If the symptoms do not resolve in a few days to two weeks for patients diagnosed with AOM, physicians prescribe antibiotics, such as amoxicillin or cefdinir [2, 4]. Over-diagnosing OM is a common issue and of widespread concern, as antibiotic resistance may rapidly develop, especially during early childhood [10]. This again reinforces the importance of an accurate diagnosis of OM. In the case of patients diagnosed with OME, physicians may perform hearing tests to determine if the MEE is inhibiting the hearing process. Performing a myringotomy (incision of the TM) to drain the fluid, or placing an ear tube (tympanostomy tube), as shown in **Figure 5**, is recommended for patients with persistent MEEs, with conductive hearing loss, or with severe earache.

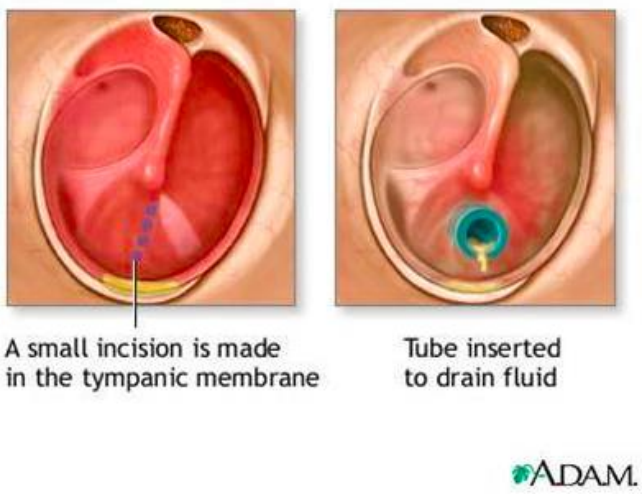

Figure 5. *Illustration of a myringotomy (incision) and tympanostomy tube to drain persistent middle ear effusions from the middle ear cavity. Photo from [26].*

The most frequent complication from OM is temporary hearing loss until the MEE is cleared from the middle ear. Pediatric patients may experience delayed learning, especially during language development stages, but OM is unlikely to cause permanent education problems [27]. Other complications such as intracranial or extracranial infections are potentially serious, but are infrequent, occurring in roughly 3.3% of untreated or complicated cases [28].

2.2 DIAGNOSIS OF OTITIS MEDIA

Otitis media is commonly diagnosed based on the otoscopic view of the TM to determine the presence of MEEs. Despite the high prevalence of OM and the frequent need to diagnose, the diagnostic accuracy for OM is surprisingly low, between 40-60%, depending on physician experience and expertise [29]. The major limitation for making this diagnosis is the qualitative information provided by standard diagnostic methods, leading to misinterpretation. Although the guidelines for diagnosing and treating OM are continually updated [4, 6], the difficulty of diagnosis remains the same because the subjective information from the diagnostic tools remains the same.

The current methods for diagnosing and monitoring OM include standard otoscopy, pneumatic otoscopy, tympanometry, and wideband acoustic immittance (WAI) measurements. In this section, the basic principle for each method is introduced, along with corresponding benefits and limitations.

2.2.1 Otoscopy

The standard method for diagnosing OM is by an otoscope, shown in **Figure 6**. The head of an otoscope contains a light source and a simple magnifying lens so that physicians can obtain surface

views of the ear canal and the TM, and determine qualitative features such as the translucency/opacity, the degree of redness (erythema), the amount of light reflectivity (or dullness), and if translucent, whether fluid is present within the middle ear cavity. The benefits of an otoscope include ease of use, high accessibility, and low-cost. On the other hand, the information is entirely qualitative, and the view behind the TM is difficult to achieve if the TM is not translucent. Furthermore, it may be difficult to observe the entire width of the TM, depending on the orientation of the ear canal, the TM, and whether any ear cerumen (wax) is present.

***Figure 6**. Standard otoscope and its representative images of the TM in normal and OM conditions. Photo from [30]*

2.2.2 Pneumatic Otoscopy

When a rubber-made pneumatic bulb is attached to a standard otoscope to induce and examine the movement of the TM, the procedure is called pneumatic otoscopy, illustrated in **Figure 7**. This diagnostic method is strongly recommended for physicians in order to confirm the presence of a MEE, as it provides higher sensitivity (94%) in detecting fluid [8, 9]. The pressure generated from

the rubber bulb is applied to the ear canal. Physicians are then able to examine the mobility of the TM in response to the varying pressure, and the position of the TM (retracted or bulging). This information may be crucial to distinguish different types of OM, as a bulging TM may indicate AOM, whereas a retracted TM may imply OME.

Figure 7*. Pneumatic otoscope. Photo from [30]*

The main advantage of pneumatic otoscopy is the capability of studying the TM dynamics with a low-cost method. In addition, this method is considered to be the most accurate among other middle ear diagnostic devices [7, 31]. However, even if detecting MEEs by pneumatic otoscopy is key to establish a diagnosis of OM, few physicians utilize this method on a regular basis due to several limitations. First of all, pneumatic otoscopy still generates qualitative images of the TM, leading to subjective interpretations based on experiences and training. Due to a lack of quantitative measures, it is often unclear if less mobility of the TM is due to a MEE, or simply the air leakage from the tool or from the ear canal. A wide range (220-1130 daPa, where 1 daPa = 10 Pa) of pressure intensity can be generated by manually squeezing the bulb, which is another reason

attributed to the high misinterpretation rate [32]. Furthermore, not squeezing the pneumatic bulb before placing the speculum into the ear (to generate negative pressure) and creating an air seal may significantly affect the results.

2.2.3 Tympanometry

A tympanometer, shown in **Figure 8**, is a commonly used middle ear diagnostic tool that acoustically examines middle ear function. The ear probe emits a sound wave with a homogeneous frequency (usually 226 Hz, but 1000 Hz for infants) in the ear canal. A pressure regulator in the device varies pressure in the ear canal through an air pump in the probe. A microphone subsequently picks up the reflected sound wave from the TM to calculate acoustic admittance, considered as an acoustic mobility of the TM. Based on the fact that the TM is most efficient in transferring the sound wave when the pressure on both sides of the TM is the same, tympanometry can measure the middle ear pressure (MEP) [33]. As a result, a tympanometer generates a tympanogram, which plots the admittance as a function of the ear canal pressure.

***Figure 8**. Standard portable tympanometer. Photo from [34]*

In addition to the ability of measuring MEP, tympanometry can help diagnose OM based on the different tympanogram traces, shown in **Figure 9**. A tympanogram is mainly categorized into three types: A, B, and C. A 'Type A' tympanogram represents a healthy middle ear condition, which contains one sharp peak admittance. Depending on the peak admittance, 'Type A' can be subdivided into 'Type As' (lower compliance) and 'Type Ad' (higher compliance), although these types are still considered as normal conditions.

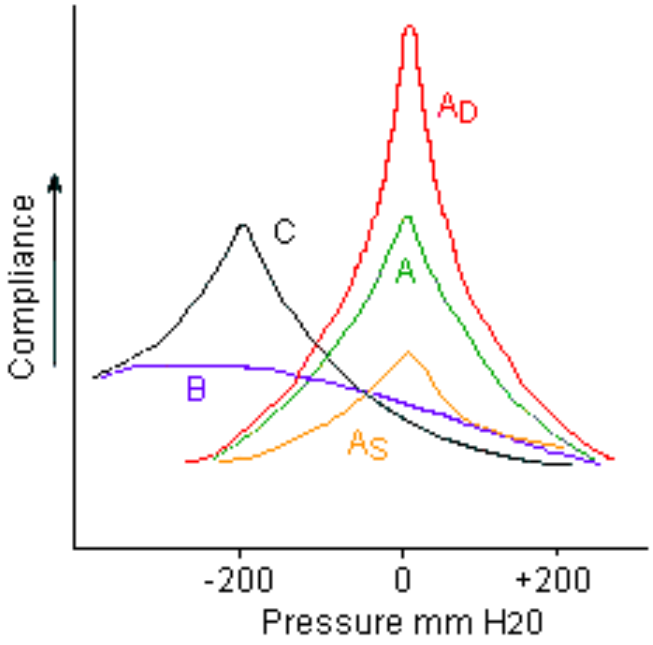

Figure 9. *Tympanograms. "Type A" tympanogram indicates a healthy middle ear condition, which can be subdivided into Type As (lower compliance) and Type Ad (greater compliance). "Type B", flat compliance, may indicate the presence of a MEE. "Type C" is considered as the transition stage from Type A to Type B, characterized by a strong negative MEP. Plot from [35].*

A 'Type B' tympanogram indicates the presence of a MEE behind the TM, suggesting that the microphone was unable to measure any reflected sound waves from the TM due to the fluid build-up in the middle ear cavity. A 'Type B' tympanogram does not include a peak; instead, the admittance is close to zero and nearly constant as the MEP is varied. Thus, neither acoustic

mobility nor the MEP can be measured from a 'Type B' tympanogram, lacking quantitative information. Furthermore, a 'Type B' tympanogram alone does not always guarantee the diagnosis of OM. The positive predictive value for OME diagnosis ranges from 49% – 99% only when used with history and otoscopy findings [33, 36, 37]. Moreover, there are other possible conditions besides MEEs that may result in a 'Type B' tympanogram. These include an immobile TM or a TM with a perforation, or impacted cerumen.

A 'Type C' tympanogram is known to signify the transition from Type A to Type B. A 'Type C' tympanogram typically contains a lower peak admittance of the TM with a negative MEP, which can be indicative of an early-stage of OM [33]. The negative MEP is often created when the gas trapped in the middle ear is absorbed by the surrounding tissues in the early-stages of OM. A 'Type C' tympanogram may be pathological, but is inconclusive as a diagnostic criterion [8, 33, 36].

Since tympanogram types cannot explicitly diagnose different types of OM, it is usually employed to confirm the presence of a MEE. The major advantage of tympanometry over standard and pneumatic otoscopy is that it provides quantitative measurements on the acoustic mobility of the TM, middle ear pressure (MEP), and ear canal volume. Nevertheless, not every physician or patient has access to a tympanometer due to the cost to purchase an instrument and be trained on the interpretation of the results. In addition, a lack of visual information is the major limitation of tympanometry, since a diagnosis of OM should not be made without visualizing the TM [10]. Another concern is the sensitivity of the normal range defined in the tympanogram. For example, of the extent of a MEE in the middle ear before a noticeable change is detected in the tympanometric data still remains questionable.

2.2.4 Wideband Acoustic Immittance (WAI)

As in tympanometry, most of the existing middle ear diagnostic tools rely on acoustic measurements to examine middle ear function, as the visualization of the middle ear cavity is limited, and acoustic responses may indicate hearing problems. One such method is wideband acoustic immittance (WAI), where WAI collectively includes all power-based acoustic measurements that mainly provide power reflectance, admittance, and impedance. First developed in the early 1990s, WAI measures the acoustic estimates of the middle ear function from wideband frequency tones (0.2 to 6 kHz, depending on the device), but without varying ear canal pressure as in tympanometry [38, 39]. One unique and advantageous quantity generated by WAI measurements is power absorption, the ratio of acoustic power reflected from the middle ear to the incident power. Power absorption can be similarly understood as an audiogram, and different trends of power absorption over wideband frequency may differentiate middle ear disorders, although a greater sample size is imperative. [40, 41].

The major benefit of WAI measurements is that it non-invasively generates functional information of the middle ear that can be interpreted in relation to hearing loss [42]. In addition, the sealing of the ear canal is not required, as in pneumatic otoscopy and tympanometry, and therefore, the accuracy of data is less dependent on this, although probe insertion is still necessary to collect the acoustic signals from the middle ear. Nonetheless, there are several limitations that challenge its use in clinical practice. First, WAI does not provide any structural information of the middle ear, the information that physicians highly prioritize when diagnosing OM. Another significant limitation is that the acoustic responses of the middle ear non-specifically and non-systematically vary depending on many parameters. The trends of power absorption will significantly change depending on the amount and the types of MEEs, MEP, types of OM, and

stages of OM [40]. However, the effect of each factor and the combined effect of these factors on WAI measurements have not yet been thoroughly studied, largely due to a lack of a gold-standard to confirm these parameters. Investigating and understanding the *in vivo* acoustic responses of the human middle ear based on animal studies and cadaveric studies may not be the most appropriate. Thus, more rigorous clinical studies are expected to fully comprehend the effect of different pathological conditions on reflectance measurements. Note that only the more commonly performed diagnostic methods and instruments are included in this thesis. Other existing methods include optoacoustic emission (OAE) and acoustic reflex measurements, which are used far less often.

2.2.5 Limitations of the Current Methodology

An accurate diagnosis of OM is intrinsically challenging because the middle ear cannot be fully assessed from the external ear non-invasively. Thus, most current methodologies rely on visually observing the TM and measuring the acoustic transmittance of the middle ear. The features of the TM, such as color, transparency, or the position, can be evaluated from otoscopy, yet they are highly qualitative. One study showed that around 30% of 135 AOM cases were falsely diagnosed as positive, in which these false positive cases were mostly indeed OME and non-OM cases [43]. Furthermore, 88% of false positive cases actually contained no MEEs, again emphasizing a low accuracy of detecting MEEs, although confirming that the presence of a MEE is necessary to establish the diagnosis of OM [43]. This percentage is surprising, as it indicates how commonly AOM is over-diagnosed, leading to an increase in the prescription of antibiotics, and increasing antibiotic resistance in the pediatric population. While the acoustic measurements from tympanometry and WAI can be quantitative methods, these measurements themselves cannot

provide sufficient information of the middle ear, as the acoustic information is an outcome of a combination of factors that are not yet fully understood. Therefore, there is an urgent need to develop a visual but quantitative diagnostic tool for OM.

2.3 OPTICAL COHERENCE TOMOGRAPHY (OCT)

Optical coherence tomography (OCT) is a non-invasive optical imaging technique first developed in the early 1990s [44]. OCT employs the basic principle of interferometry (commonly in a Michelson interferometer configuration) to acquire depth information of the sample from the interference signal between the reference and the sample path. The low coherence length of the light source allows for the capability to acquire depth-resolved information of the sample, and with an appropriate scanning mechanism, 2D cross-sectional and 3D volumetric images can be generated. OCT is an interesting optical imaging modality, as the axial and lateral resolutions of the system are independently determined. In addition, the non-invasive nature of OCT opens a wide variety of clinical applications, including ophthalmology, dermatology, cardiology, and oncology. In this section, the basic theory of OCT is explained, and clinical applications of OCT in primary care medicine are introduced.

2.3.1 Basic Theory

Low coherence interferometry (LCI) using a Michelson-type interferometer is the fundamental measurement technique of OCT, shown in **Figure 10**. As the name suggests, low coherence light is used as the light source. The beam splitter in a free-space system or the fiber coupler in a fiber-based system splits the incident light from the low coherence light source and sends it into two paths: a reference arm and the sample arm. A mirror is typically placed in the reference arm. The

back-reflected electric fields from the mirror and the sample are combined by the beam splitter or the fiber coupler and detected as the short-time-averaged light intensity. When the path lengths in the two arms are matched, meaning that the optical path length difference between two arms is within the coherence length of the light source, an interferogram that carries depth information of the sample is created. The back-scattered signals are recombined and measured by a detector. The envelop of the interferogram in the detected signal is extracted and converted to one-dimensional depth-resolved information, called an A-scan. Acquiring A-scans over a spatial distance and/or a period of time can generate a multi-dimensional or/and volumetric OCT image, such as B-scan (A-scan over distance), M-scan (A-scan over time), or BM-scan (B-scan over time). Several important mathematical expressions are described herein.

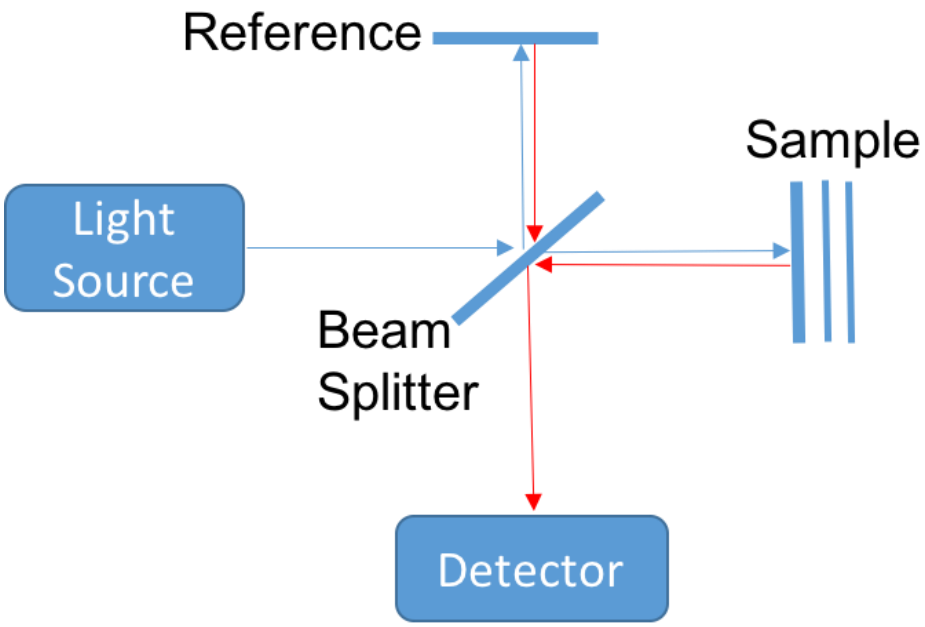

Figure 10. *Basic schematic diagram of an OCT system based on a Michaelson-type interferometer with reference and sample arms.*

At the detector, the resulting light intensity, *I(t)*, is represented as:

$$I(t) = <| E_R + E_S |^2>, \qquad (1)$$

where the backscattered electric field E of the beams can be defined as:

$$E_R = E_{R0} \exp(i(2k_R l_R - \omega t)) \quad (2)$$

$$E_S = E_{S0} \exp(i(2k_S l_S - \omega t)). \quad (3)$$

The terms E_{R0} and E_{S0} are the electric field amplitudes of the beams incident down the two paths, the reference and sample arms, respectively. The terms k_R and k_S are the propagation constants in the two beams, and l_R and l_S denote the physical length of the two arms. The terms ω and t represent the optical angular frequency and time. Substituting **Equation (2)** and **(3)** into **Equation (1)** yields a general expression of the intensity at the detector, which includes the interference signal:

$$I(t) = E_{R0}^2 + E_{S0}^2 + 2E_{R0}E_{S0} \cos(2k_S l_S - 2k_R l_R). \quad (4)$$

The first two terms are often known as 'DC (direct current)' terms, which depend on the initial light intensity entering the two arms. The last term is known as 'AC (alternating current)' term, which carries the actual interference fringe signal based on the two arms. When k_R and k_S are equal, the phase difference, $\Delta\phi$, can be written in terms of the path-length difference, Δl, between the two arms:

$$\Delta\phi = 2k(l_S - l_R) = 2k\Delta l = 2\pi \frac{2n\Delta l}{\lambda_0}, \quad (5)$$

where n is the refractive index and λ_0 is the center wavelength in a vacuum. Again, the coherence length of the light source determines the window that the interference signal can be generated.

Thus, the coherence length of the light source determines the axial resolution of the OCT system by the Wiener-Khinchin theorem, stating that there is a Fourier relationship between the

autocorrelation function (G) of the electric field and the Gaussian-shaped power spectrum of the light:

$$\int_{-\infty}^{+\infty} G_1(\tau)\exp(i\omega\tau)d\tau = |E(\omega)|^2 = S(\omega) = \frac{1}{\sqrt{2\pi}\sigma_\omega}\exp\left(-\frac{(\omega-\omega_0)^2}{2\sigma_\omega^2}\right), \quad (6)$$

where ω_0 is the center angular frequency and σ_ω is the standard deviation of ω. Normalization of the source spectrum, S, gives the coherence length in terms of the source parameters, and thus the axial resolution in air, Δz, is defined as:

$$\Delta z = \frac{4\ln 2}{\pi n}\frac{\lambda_0^2}{\Delta\lambda}. \quad (7)$$

The ability to provide high-resolution depth-resolved information is a major advantage of OCT. In addition, OCT provides independent axial and transverse, or lateral, resolution, unlike other optical imaging modalities such as confocal microscopy. The axial resolution is directly related to the coherence length of the light source, l_c, thus proportional to the center wavelength of the source, λ_0, but inversely related to the square of the bandwidth of the light source, $\Delta\lambda$, as expressed in **Equation (7)**. On the other hand, the focusing optics in the sample arm primarily determine the field-of-view as well as the lateral resolution. The lateral resolution of OCT depends on the focal length of the focusing lens in the sample arm, f, and the beam diameter, D, incident on the lens, as follow:

$$\Delta r = \frac{4\lambda_0}{\pi}\frac{f}{D} \approx \frac{2\lambda_0}{\pi}\frac{1}{NA}. \quad (8)$$

In general, the axial resolution of OCT ranges from 1-10 μm with few millimeters of imaging depth. By scanning different region over the sample, OCT enables 3D volumetric imaging of the sample with high-resolution.

Since the early 1990s, OCT has evolved with different scanning mechanisms and functionalities to maximize its potential uses in biomedical imaging. OCT is mainly categorized into time-domain OCT (TD-OCT) and frequency-domain OCT (FD-OCT) systems. In TD-OCT, the depth information of the sample at different depth is acquired by periodically oscillating the reference arm path length over the distance of depth of focus in the sample arm. The mirror on the reference arm is often controlled via a mounted mechanical galvanometer. Thus, the acquisition speed is limited by the mechanical speed and inertia of the galvanometer. Only when the path-length difference is within the coherence length of the source, the interference signals are detected by the photodetector, and by varying the reference arm path length, various depths within the tissue (in the sample arm) are probed.

FD-OCT utilizes spectral interferometry, and can be subdivided into spectral-domain OCT (SD-OCT) and swept-source OCT (SS-OCT). In SD-OCT, a spectrometer composed of the dispersive materials and a line scan camera is utilized to acquire spectral information, instead of mechanically varying the reference arm path-length as in TD-OCT. Therefore, the acquisition speed depends on the acquisition rate of the spectrometer. The spectral interferograms at the detector are converted to A-lines (single depth-resolved scans) by taking the inverse Fourier transform of the interferogram. Detailed methods for post-processing of raw OCT data are described in Chapter 4. On the other hand, SS-OCT utilizes a photodiode as a detector, and employs a light source that can quickly sweep a range of frequencies to measure the various spectral components. Overall, FD-OCT provides a faster frame rate and a higher sensitivity than TD-OCT, as all backscattered light is detected at the same time in FD-OCT. In this thesis, an LCI imaging system based on Fourier domain detection was developed.

2.3.2 OCT from Benchtop to Bedside

Since the development of OCT, there has been a surge of OCT investigations for biomedical applications, mainly for the diagnosis and monitoring of diseases. In translational research, the transition from the laboratory benchtop to the patient bedside is critical. OCT systems built in research settings have been re-engineered for clinical studies, yet still must maintain high imaging performance and high image acquisition speed. Requirements for a bedside OCT imaging system include: high portability, durability, stability, compact size, rapid acquisition and processing of the images, and ease of use for physicians and nursing staff. More importantly, the objectives and specifications of the system should be designed based on the specific clinical application. For example, the sample arm of the system can include a handheld probe, a fiber-based probe for a catheter or endoscope, or a probe with an articulating arm [45]. In addition, technological advances in optical communications and data sciences have developed enhanced laser sources, beam delivery methods, detections schemes, data storage, and analysis [46]. With improved hardware and software, OCT systems have quickly and continuously been developed for different clinical settings, ranging from a typical outpatient clinical exam room to the surgical suite, and for various medical applications including in ophthalmology, cardiology, dermatology, gastroenterology and oncology, to name only a few [46, 47].

2.3.3 OCT in Primary Care Medicine

OCT has been rapidly employed for clinical research after its development and evolution as a bedside imaging technique due to several advantages over currently available imaging modalities. OCT enables higher resolution imaging compared to X-ray CT and MRI, which provide sub-millimeters of resolution at best, utilizes label-free contrast (scattering properties of tissue) with

high sensitivity, and costs considerably less than X-ray CT and MRI. In addition, a low-power low-coherence light source for OCT is safe, contrary to ionizing imaging techniques, such as X-ray CT and nuclear imaging. The speed of image acquisition is also comparably fast and three-dimensional images can be generated. Although these unique characteristics have enabled various clinical OCT studies, the use of OCT for primary care imaging is relatively new, representing a front-line imaging technique common in any medical care.

Comprehensive screening in primary care offices is critical for patients to receive appropriate and effective treatment and referral, and to decrease the cost of care [48]. Nonetheless, diagnostic tools in primary care offices, including an otoscope and ophthalmoscope, remain almost the same since their development over a hundred years ago, limiting an accurate and early-diagnosis of diseases at the front-line. To provide depth-resolved information from different tissue sites, ranging from the eye, skin, oral cavity, and middle ear, a handheld OCT system for primary care physicians was developed, shown in **Figure 11**. [49, 50]. OCT systems have allowed quantitative measurements and showed potential as an accurate early-diagnostic tool for many diseases that can be examined in primary care offices, including diabetic retinopathy, macular edema, skin cancer, and OM [49, 50]. In this thesis, the focus is on middle ear imaging and diagnostics in primary care medicine.

Figure 11*. Primary care imaging with an OCT system and handheld imaging probe, imaging a child's middle ear in a mock exam room.*

OCT was first used for human middle ear imaging in 2001, although the measurements were performed on a cadaveric human ear [51]. Since then, OCT has been employed as a prospective middle ear diagnostic and monitoring tool during middle ear surgeries [49, 50, 52-54]. With greater interests in real-time clinical imaging of the human middle ear, a recent paper summarized the requirements of OCT systems for middle ear imaging, including low NA (<0.022), system sensitivity (> 97 dB) and dynamic range (> 61 dB) to satisfy design challenges in clinical settings [52]. Our previous studies have developed portable and handheld LCI and OCT systems to visualize the human TM and MEE *in vivo*, and showed that OCT can generate quantitative structural and mechanical information, including TM thickness, MEE and biofilm presence, and MEE viscosity in the middle ear [53-56]. A more recent study showed the development of an LCI system with pneumatic function using a piston, demonstrating the measurements of the pneumatic-induced motions of the TM in adults [57]. These studies showed the potential of OCT middle ear

imaging not only for primary care medicine, but also for specialized care in otolaryngology, as OCT can generate greater information of the middle ear structures and dynamics. Besides these advances in OCT middle ear imaging, other optical methods have also been applied to standard otoscopy and middle ear imaging in order to overcome the limitations of traditional otoscope-based diagnostic methods.

2.4 RECENT STUDIES OF OPTICAL MIDDLE EAR IMAGING

Developing non-invasive middle ear imaging techniques has been of great interests for many researchers in the field of otolaryngology and medical imaging, due to the anatomical limitations associated with visualizing the middle ear space *in vivo*. In this section, recent advances of clinical middle ear imaging with OCT are described. Furthermore, several studies on optical middle ear imaging, not limited to OCT, are briefly reviewed.

2.4.1 Tympanic Membrane Mapping using OCT

As the TM plays an important role in middle ear function, it is valuable to identify early- changes in properties of the TM, such as shape, thickness, viscoelasticity, and other mechanical properties, during an ear examination [58]. The thickness distribution of the TM may be crucial when diagnosing OM, as the TM might thicken as a result of inflammation [4], or from the formation of biofilm [59].

The capability of OCT to non-invasively generate cross-sectional images of the tissue allowed precise measurements of the thickness distribution of the TM *in vivo* [60]. In addition, a 3D model of the full-field TM was reconstructed from OCT measurements [58], and a mosaicking approach to generate a map of the TM was developed using LCI measurements [61]. Although the

thickness measurements largely vary spatially and are based on each individual subject, the range of roughly 70-100 μm can be considered as an average thickness of the TM from OCT measurements, which also has been correlated with histology [58]. These studies proved that the morphological and geometrical parameters in the TM can be accurately measured by OCT *in vivo* and non-invasively.

2.4.2 Middle Ear Cavity Imaging using OCT

Although OCT can provide cross-sectional, depth-resolved images of the TM, it cannot provide an entire view of the middle ear cavity due to its limited penetration depth from tissue scattering and absorption. The intrinsic geometry of the human middle ear is the major challenge; the TM diameter of 10 mm and a relatively large middle ear volume require OCT systems to have a wide scanning range with a greater imaging depth [52]. Nevertheless, one study generated images of a greater volume of the middle ear cavity by collecting the signals from two different focal planes and angular orientations [62]. This probe combined phase sensitive OCT and a video otoscope, visualizing the ossicles. However, the sensitivity and the contrast of the images still needed to improve for translational studies.

The imaging depth can be further improved by utilizing swept-source OCT (SS-OCT). A preliminary study investigated *in vivo* human middle ear cavity imaging with SS-OCT, although the ossicles were visible from only 50% of subjects and the clinical significance has not yet been assessed [63, 64]. However, with rapid advances of swept-source laser technologies, SS-OCT may be feasible to visualize the middle ear cavity *in vivo.*

2.4.3 Non-OCT Optical Middle Ear Imaging

Besides OCT, several recent studies have developed different optical imaging methods to better visualize middle ear pathologies with enhanced resolution, field-of-view, and depth-of-field. Such examples include light-field imaging [65], infrared imaging [66], fluorescence imaging [67], and holographic imaging [68], and each method is briefly described herein.

A light field image reconstructs a 3D map of the sample by collecting multi-view images achieved by a micro-lens array [69]. Bedard et al. developed a light field otoscope that generated 3D images of the TM from a single-snapshot, with a depth precision of 0.06 mm of ground truth values. Although the positions (bulging, neutral, or retracted) of the TM were visualized from the 3D maps, the imaging depth was too shallow to detect the presence of MEEs, and only provides a partial view of the middle ear cavity.

Visualization of MEEs with shortwave infrared (SWIR) light was another noteworthy finding, as MEEs showed a strong absorption of the SWIR light between 1400-1550 nm, thus appearing black in the image [66]. This optical contrast was primarily due to the water content in the MEEs. Furthermore, imaging with longer wavelengths allowed for deeper imaging of the middle ear, visualizing ossicles, cochlear promontory, and the round window niche. However, differentiating each middle ear structure from one 2D projected image can be demanding and the effects of different types of MEEs are unknown. Clinical studies with different middle ear pathologies will be essential to validate the significance of this unique optical contrast.

A fluorescence otoscope utilizing multiple wavelengths for excitation was developed to detect autofluorescence signals from middle ear structures [67]. These chemical and spectroscopic measurements generated functional information from different tissue compositions (collagen, NADH, FAD and keratin) and biochemistry from the TM and middle ear. *In vivo* imaging of

cholesteatomas (metabolically more active than normal) was investigated and the authors claim that detected signals will be different for cases with MEEs during OM. Nonetheless, an *in vivo* clinical study has not yet been performed for subjects with OM, and having a real-time, wide-field imaging capability will be necessary for further clinical applications.

A holographic otoscope measuring nanoscale displacements of the TM was developed to show the potential of the system for quantifying the acoustic-induced deformation of the TM. Nanometer resolution was achieved by detecting the differences in optical phase of two stimuli based on phase-shifting digital holography [68]. This system can be used in a non-contact mode with full field of view covering the TM. The viscoelasticity of the TM was also modeled. However, the measurements were only shown from a post-mortem chinchilla TM without the external ear canal, and *in vivo* clinical studies in otology are likely to be significantly more challenging and problematic.

3 SPECIFIC AIMS

Despite the high prevalence of OM, middle ear dynamics in relation to OM is not yet thoroughly understood. Even the diagnosis of OM alone is intrinsically challenging, leading to uncertainty and incorrect treatments. The development of a new tool to better investigate OM is crucial for physicians, as it might increase the accuracy of OM diagnosis and help the management of OM. The TM has been considered as the key structure of the middle ear to examine for the diagnosis of OM. In addition, examining pneumatic TM mobility with a pneumatic otoscope is strongly recommended, since decreased mobility may indicate the presence of MEEs, and the positions of the TM may indicate the relative MEP [4, 6]. Nevertheless, the subjective assessments are difficult to interpret, and the procedure is believed to be inconvenient and difficult to perform correctly [8, 9]. Moreover, sufficient guidance on the skillful use of pneumatic otoscopy for physicians in training still needs improvement [70].

Although a few studies have quantitatively examined pneumatic-induced motions of the TM using video otoscopy [71, 72], no clinical studies have directly measured the TM displacements in response to pneumatic stimuli *in vivo*, mainly due to a lack of non-invasive imaging techniques. Therefore, there is a clear need to quantitatively and non-invasively assess pneumatic mobility of the TM and OM-associated middle ear dynamics. By utilizing LCI, an objective measurement of the TM mobility and middle ear dynamics may help characterize different pathological conditions, potentially creating new parameters to assess the middle ear conditions for physicians and clinical researchers. Therefore, the three primary aims of this research are:

3.1 **AIM 1:** To develop a pneumatic LCI system with an automated pressure generation module.

Our previously designed pneumatic LCI system [57] showed the capability of directly measuring TM displacement when pressure transients were applied to the TM. However, the measurements were only performed in adult subjects, and the piston was manually controlled to generate pressure transients. Since only positive pressure was applied to the TM, the capability of the system to examine middle ear dynamics was limited. Thus, it is essential to implement an adjustable and automated pressure generation system that can create both positive and negative pressure to quantitatively examine both a bulging and retracted TM.

3.2 **AIM 2:** To develop pneumatic LCI metrics that can represent TM dynamics.

The pneumatic LCI system used in this research collects entire traces of the TM displacement and the simultaneous pressure measurements over time. As a diagnostic tool, the information often needs to be concise and easy to interpret for physicians to make a diagnosis in a short period of time. Thus, defining simple quantitative metrics that can represent the essential middle ear conditions is vital.

3.3 **AIM 3:** To acquire *in vivo* pneumatic LCI measurements and compare with tympanometry.

In order to assess the clinical significance of the quantitative metrics, measurements from subjects with different pathological conditions need to be acquired. Moreover, a comparison with current middle ear diagnostic tools will not only help interpret and validate the quantitative metrics, but also evaluate our pneumatic LCI system. Therefore, the acoustic mobility and MEP determined

from tympanometry will be compared with the pneumatic LCI metrics, along with physician diagnosis, to reinforce the clinical significance of the quantitative metrics.

4 METHODS

In this section, systematic, experimental, and analytical methods of the research are explained in detail so that the measurements can be shown to be reproducible.

4.1 SYSTEMATIC METHODS

The systematic methods of this research approach include the schematics used in building the pneumatic LCI system, focusing more on developing an automated pressure generation. The system characterization methods of the pneumatic LCI system are also included.

4.1.1 Development of Pneumatic LCI System

For this study, our custom-built pneumatic LCI system was modified from a previous generation [57] to create automated and adjustable pressure transients (pressure intensity of ±150 daPa and a total duration of 0.5 sec) using a voice coil (LCAM 5/15, H2W Technologies,) and a standard pneumatic bulb. The overall system schematic is illustrated in **Figure 12**. The system is largely divided into three parts: 1) base module, 2) handheld probe, and 3) pressure module.

In the base module, a super-luminescent diode light source with a center wavelength of 940 nm and a bandwidth of 70 nm (Broadlighter S930, Superlum), a spectrometer (C940-UDC, Wasatch Photonics, maximum A-scan rate of 40 kHz) as a detector, a computer for acquiring and processing the data, and a reference arm of the LCI system are encompassed.

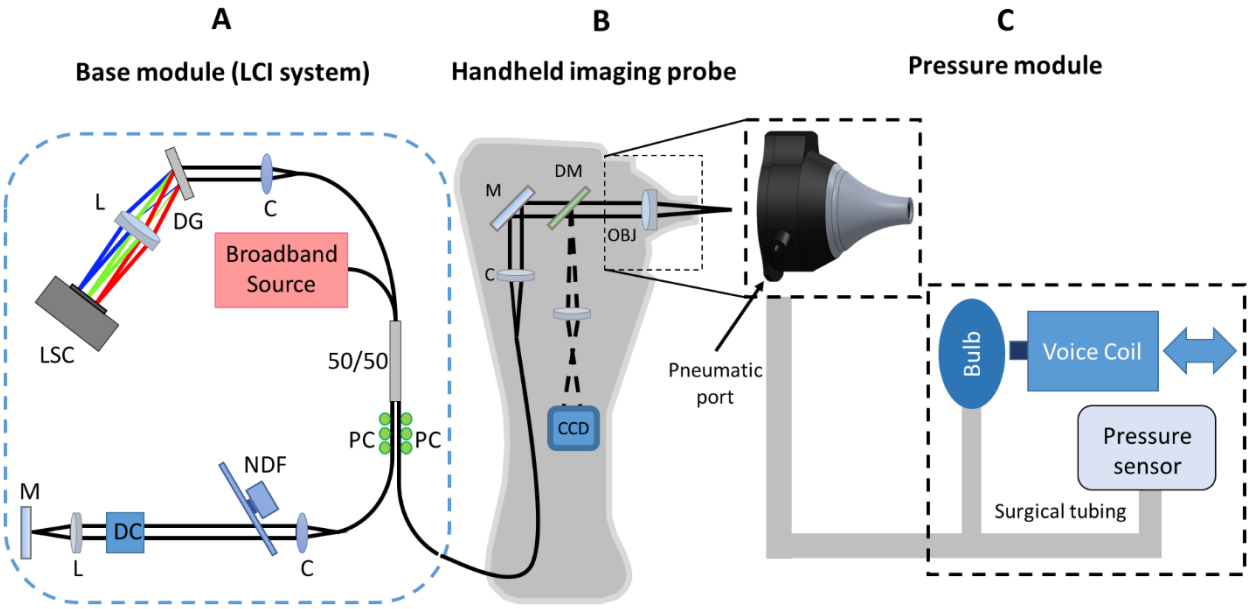

Figure 12. *Schematic diagram of pneumatic LCI system. LSC: line scan camera, L: lens, DG: diffraction grating, C: collimator, 50/50: fiber coupled beam splitter, PC: polarization controller, NDF: neutral density filter, DC: dispersion compensation, M: mirror, DM: dichroic mirror, OBJ: objective lens, CCD: charge-coupled device camera.*

The sample arm of the LCI system connects the base module and the handheld probe. The 3D printed probe encompasses a near-infrared light path for the sample arm, and a visible light path for the camera imaging, separated by a dichroic mirror. A mini camera with USB interface (MU9PC-MH, Ximea) was utilized to acquire RGB otoscopic views of the TM, simultaneous with the LCI M-scans. The use of an otoscope head with a pneumatic port from a commercially available standard otoscope allowed for the use of standard Welch-Allyn ear specula and pneumatic bulb. An objective lens in the sample arm (f = 70 mm) was used to both focus the beam onto the sample and to seal the space in the otoscope head.

The pneumatic port of the handheld probe was connected to a thin surgical tube attached to the pressure module, where most improvements over the previously designed pneumatic LCI

system were made. The automated pressure stimuli were produced by the voice coil compressing the pneumatic bulb inside the pressure module. A simple circuit composed of resistors, capacitors, a push-button switch, a pressure sensor (SSC Series, Honeywell), and a potentiometer was implemented into the module, shown in **Figure 13**. The user can control the amplitude of the pressure transients by the potentiometer, such as for gentler (less than 100 daPa) stimuli for pediatric subjects. Rapid pressure transients can also be delivered using a push-button switch. The capacitors and a mechanical stopper were also used to prevent any unexpected high amplitude pressure forces from the moving voice coil. The pressure from the pneumatic bulb was applied to the ear via the pneumatic port of the handheld probe, and was simultaneously measured using the miniature board-mounted pressure sensor. A rubber earbud was attached to a disposable ear speculum to seal the ear canal. The use of a standard pneumatic bulb was beneficial, as it generated similar pneumatic responses of the TM as in standard pneumatic otoscopy, which could then be quantified with LCI.

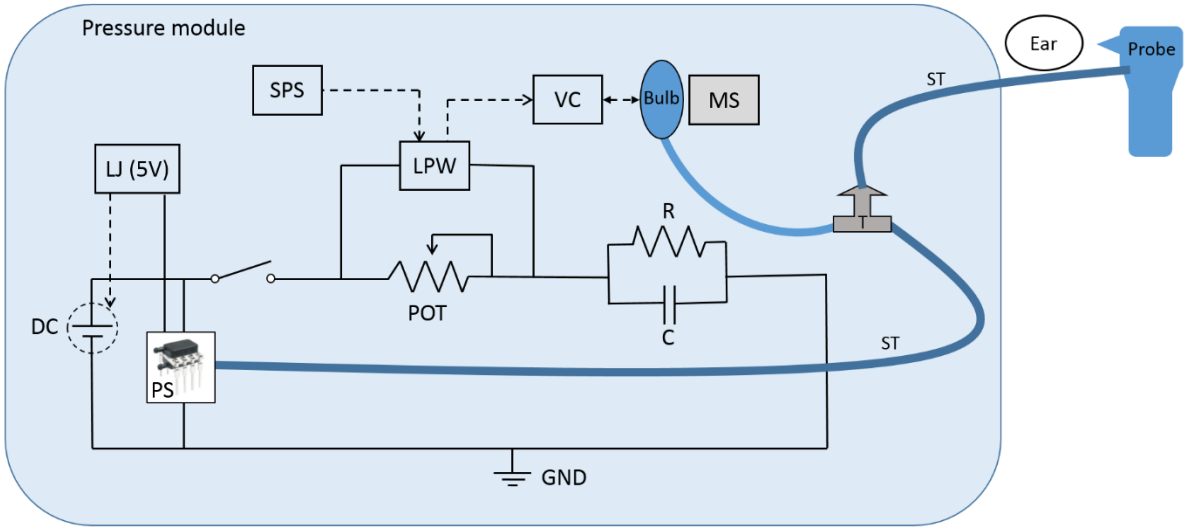

Figure 13. *Circuit diagram of the pressure module. DC: DC power supply, LJ: Labjack, PS: pressure sensor, SPS: switching power supply, LPW: linear power amplifier, POT: potentiometer (0-25 kΩ), GND: ground, VC: voice coil, MS: mechanical stopper, R: resistor (50 kΩ), C: capacitor (100nF), T: T-shape connector, ST: surgical tubing.*

As a result, the overall pneumatic LCI system allowed for both imaging and measurements in an outpatient clinic exam room (See **Figure 14**).

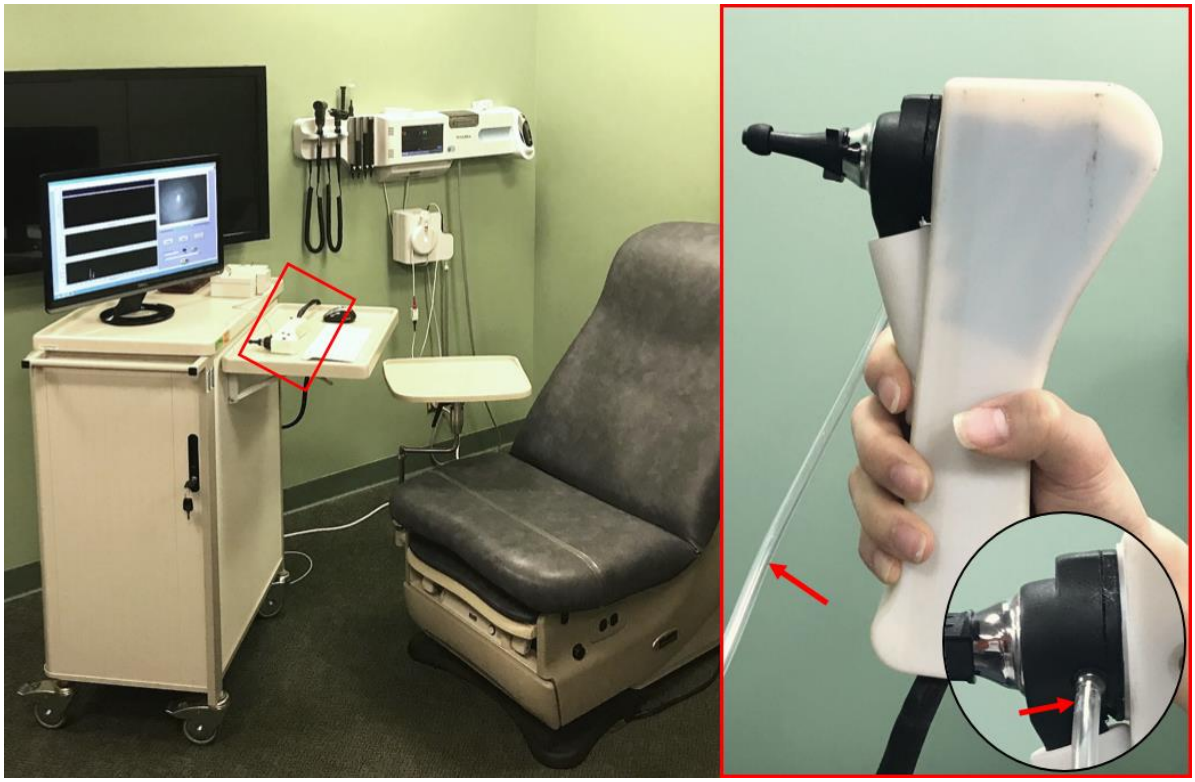

Figure 14. *Pneumatic LCI system in a mock exam room. Photo on right shows zoomed in handheld probe. The handheld probe uses a standard ear speculum with a rubber earbud to ensure a pressure seal within the ear canal. The pneumatic pressure stimulus is provided via a pneumatic port (bottom right) and surgical tube (red arrows).*

4.1.2 System Characterization

To characterize the pneumatic LCI system, the axial and the lateral resolution were measured with a mirror placed in the sample arm. The theoretical axial resolution by Equation (7) was computed to be 5.6 μm in air. The point spread function (PSF) of the system with a mirror at the focal plane of the sample arm optics is shown in **Figure 15**. Based on the full-width-half-maximum (FWHM) of the PSF, the measured axial resolution of the system in air was determined to be 6.5 μm. The numerical aperture (NA) of the focusing optics in the sample arm resulted a lateral resolution of

20 µm. The temporal resolution depends on the A-scan rate of the spectrometer and the acquisition speed of the pressure measurements, both determined to be 1 msec.

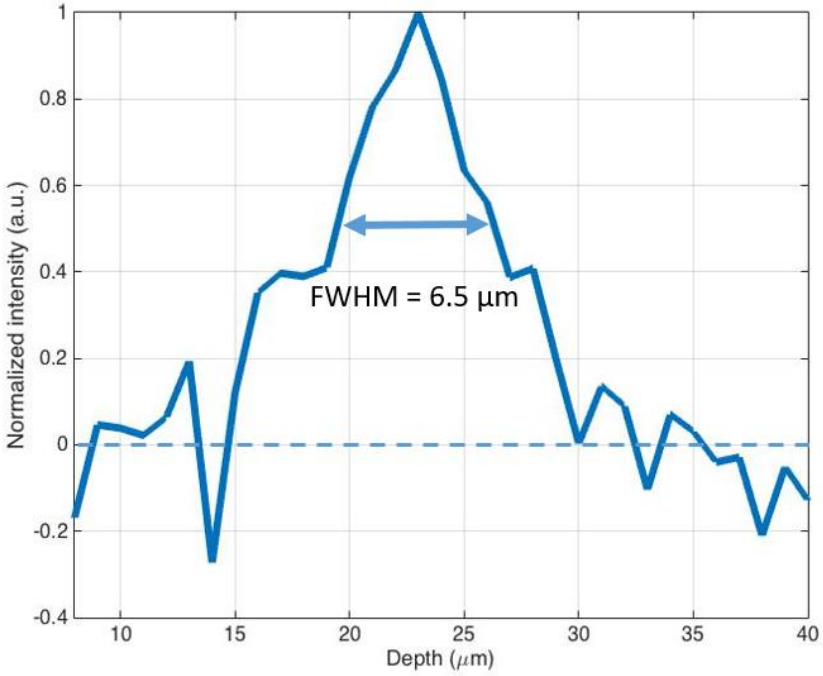

Figure 15. *Point spread function (PSF) of the pneumatic LCI system. Note that after converting the vertical axis (intensity) to the logarithmic scale, the horizontal axis (depth) was zoomed in for visualization purpose, and the signal was divided by the maximum intensity for normalization. Dotted line indicates averaged noise signals.*

4.2 ANALYTICAL METHODS

The analytical methods include the data acquisition and post-processing of LCI and the pressure measurements. The quantitative metrics for the system are defined, and statistical methods to evaluate clinical significance of the metrics are described.

4.2.1 OCT Data Acquisition and Processing

The pneumatic LCI system acquired M-scans for 2 seconds. A spectrometer with 4096 pixels and a spectral resolution of 0.02 nm/pixel (C940-UDC, Wasatch Photonics) was utilized at an A-scan rate of 1 kHz. The system employed frame grabbers (PCIe-1473R, National Instruments) to store

and transport the data from the spectrometer to the computer. Real-time OCT data processing was performed by LabView (2012) via the following steps: 1) reshape of raw data based on image width and height, 2) subtraction of DC component based on the background measurement (intensity measured without any sample), 3) dispersion correction, 4) fast-Fourier transform, and 5) conversion to logarithmic scale to further enhance the image contrast. The processed M-scans were displayed on a monitor with the RGB surface view of the TM so that the user could efficiently acquire the depth information at a point of interest.

The pressure measurements were simultaneously performed as LCI measurements. In addition to the pressure sensor, an additional A/D interface (U12, LabJack) was employed to acquire the pressure measurements. A foot trigger was also implemented to initiate the data acquisition process. The voltage signals from the pressure sensor were converted to the pressure measurement (in mmHg) based on the calibrated data. The converted pressure signals were displayed on the monitor along with the processed LCI M-scans and the surface image of the TM.

4.2.2 Pneumatic LCI Metrics

The pneumatic LCI system recorded M-mode images at one spatial position on the TM when pressure transients were applied to the TM. At the same time, the pressure measurements were also acquired. The traces of the TM position were determined from the maximum intensity of each A-scan in the M-mode image. The TM displacements were then calculated from the traces, where zero displacement was noted as the average position of 200 A-scans immediately prior to the pressure transients. Simple quantitative metrics that can represent the pneumatic mobility and the MEP were developed based on the TM displacement and the pressure measurement:

$$\text{compliance} = \frac{\text{displacement}_{MAX}}{|\text{pressure}|_{MAX}} \tag{9}$$

$$\text{amplitude ratio} = \frac{(+)\text{displacement}_{MAX}}{(+)\text{pressure}_{MAX}} \cdot \frac{|(-)\text{pressure}|_{MAX}}{|(-)\text{displacement}|_{MAX}}, \tag{10}$$

where (+) and (-) indicate the measured positive and negative displacements of the TM, and the (+) and (-) pressures. The unit of compliance is μm/mmHg, while the amplitude ratio is unit-less.

4.2.3 Statistical Analysis

It is hypothesized that the compliance indicates the pneumatically-induced TM mobility, while the amplitude ratio is associated with the ratio of MEP relative to pressure in the ear canal. It is thus expected that the decreased mobility of the TM in OM patients can be quantified by the compliance. Furthermore, the MEP that is responsible for the bulging or retracted TM may be estimated from the amplitude ratio. To validate this hypothesis, pneumatic LCI metrics were correlated with the peak acoustic admittance and MEP determined by tympanometry using a linear regression (least-squares fit). The two metrics of each diagnostic group (based on physician diagnosis and tympanogram types) were statistically compared using the Welch's *t* test via MATLAB® to examine the potential of the metrics for determining the presence of a MEE and estimating the MEP.

4.3 EXPERIMENTAL METHODS

The detailed methods for phantom studies, and clinical studies with adult and pediatric subjects are discussed herein. Phantom experiments were performed with an anatomically similar ear model (Nasco Life/form®), shown in **Figure 16**. The ear model contained a 10 μm-thin plastic film as the TM phantom and a middle ear cavity molded from rubber.

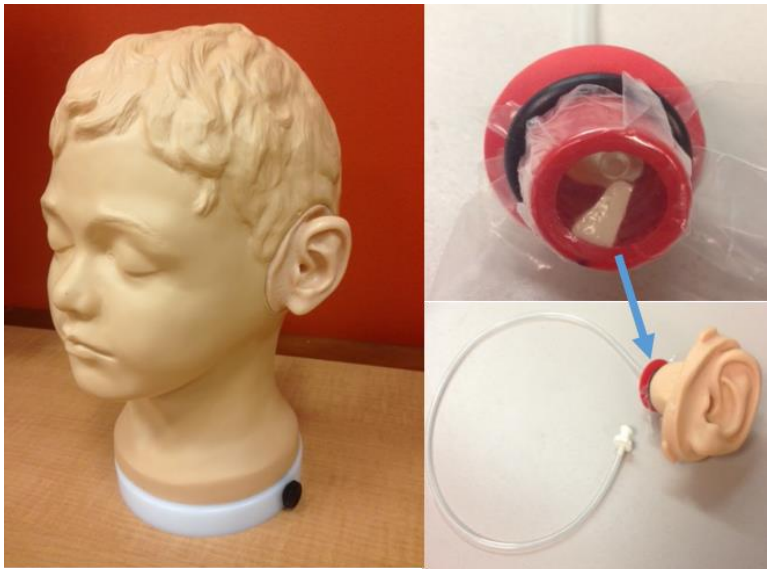

***Figure 16**. Ear model for phantom experiment. The middle ear cavity model can be filled with water or more viscous liquids. The TM is simulated by the thin plastic film (top-right).*

4.3.1 Effect of Input Pressure Parameters on Phantom

In order to test an appropriate range of the system input parameters, and to examine the effect of pressure stimuli parameters (pressure intensity and frequency of the stimuli) on the pneumatic compliance, three phantom groups (simulated normal, fully filled simulated serous MEEs (water), and simulated thicker TM group with two thin films) were generated. Tap water (viscosity of 1 cP) and petroleum jelly (viscosity of 64000 cP) were used to mimic the extreme cases of serous and mucoid MEEs, respectively, as the viscosity of MEEs varies widely from 1 to 10000 cP, with some cases over 32000 cP [73]. When the fluid was fully filled in the middle ear cavity model, the fluid was in contact with the simulated TM (film). Pressures (one period of sinusoidal-like wave with maximum intensity ranging from 5 to 50 mmHg and consistent frequency of roughly 2 Hz) were applied to three phantom groups, and the compliance after each pressure stimuli was calculated based on **Equation (9)**. This specific range of pressure intensity was chosen as the pressure greater than 50 mmHg may create severe discomfort.

Next, the effect of the pressure transients' frequencies was investigated by applying continuous sinusoidal-like pressure stimuli, with varying frequencies of 1 to 50 Hz but constant intensity of roughly 12 mmHg. The compliance was compared among different frequencies to verify that the effect of waveform frequency on compliance measurements is negligible. To generate a range of frequencies, a function generator was utilized to activate the voice coil instead of the DC voltage from the LabJack interface. Here, the effect of resonance frequency of the TM was not considered, as the TM non-uniformly resonates with a higher range of frequency, from few hundreds to 2 kHz [74]. The representative sinusoidal-like pressure stimuli are shown in **Figure 17**.

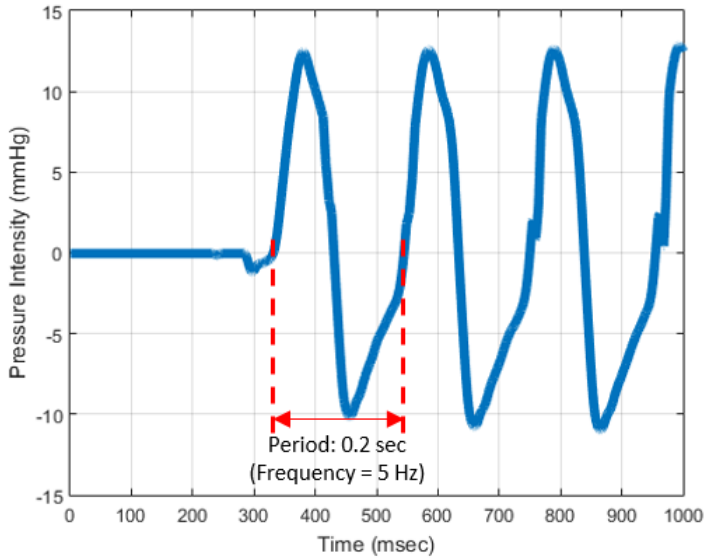

Figure 17. *Representative continuous pressure stimuli with frequency of 5 Hz and maximum pressure intensity of 12 mmHg generated from the function generator. In the case of DC voltage, one period of the pressure stimulus is applied.*

4.3.2 Effect of Amount and Types of MEEs on Phantom

After an appropriate range of pressure intensity and frequency was determined from the previous phantom experiment, it was necessary to simulate more diverse middle ear conditions that can mimic *in vivo* clinical situations. To examine the effect of different amounts and types of MEEs

on the compliance, five different conditions (simulated normal, partially filled simulated serous and mucoid MEEs, fully filled simulated serous and mucoid MEEs) were measured by the pneumatic LCI system (n=13 for each group). The phantom middle ear cavity was not pressurized for this experiment. It is hypothesized that the compliance will be less as the viscosity of the fluid increases, and the amount of fluid increases, due to the greater mass. The amplitude ratio was not tested for the phantom, as the different compliances in the opposing direction were only observed from human measurements.

4.3.3 Clinical Studies

Prior to clinical studies with pediatric subjects at a local hospital, a healthy adult volunteer was imaged by the pneumatic LCI under a protocol approved by the Institutional Review Board (IRB) at the University of Illinois at Urbana-Champaign in order to: 1) determine the repeatability of the measurements, and 2) determine if the metrics depend on the spatial location on the TM. Pneumatic LCI measurements were acquired at different spatial locations over the entire TM, and the compliance from **Equation (9)** was computed from each quadrant of the TM. Optimally, the variability of the measurements would be minimal, although spatially-varying measurements were expected due to the spatially-varying thickness and the shape and contours of the TM.

Next, to assess clinical significance of the pneumatic LCI measurements, a total of 30 pediatric subjects were recruited for a study under an IRB protocol approved by both the University of Illinois at Urbana-Champaign and Carle Foundation Hospital (Urbana, IL). Subjects were randomly selected from the outpatients visiting the primary care clinic at Carle Foundation Hospital, and the average age of these subjects was 9 ± 4 years. The proper informed consent and assent were collected. There were no exclusions based on gender, race, or ethnicity. A total of 42

ears clinically diagnosed as normal (n=25), with OM (n=10), and with upper respiratory infection (URI) without MEE (n=7) were imaged for the study. Subjects with a URI without MEEs formed an independent group (neither normal nor OM), as the symptoms of URI largely overlap with OM, while the presence of a MEE was not identified. The measurements were safe, as the pneumatic LCI system performed non-invasive imaging using low-power near-infrared light, and the maximum pressure stimuli was 250 daPa, approximately half of the maximum pressure swept by tympanometry.

The experimental procedures are described herein. After physician examination, RGB color images of the TM were acquired using a video otoscope (Welch-Allyn). Next, standard tympanometry (TM-286 at 226 Hz, Welch-Allyn) was performed to validate the hypothesis that the amplitude ratio measured from pneumatic LCI can estimate the relative MEP. Pneumatic LCI was then employed to trace the pneumatic-driven responses of the TM, along with the recorded pressure changes in the ear canal. An ear speculum with a rubber earbud tip was utilized for each ear, and disposed of after each use. Physician observations, diagnosis, and medical record notes, without any identifiable information, were collected for the subjects. The entire imaging and measurement session required around 5 minutes per ear, and was performed in an exam room.

5 RESULTS

5.1 OVERVIEW

The pneumatic LCI system was developed to quantify the TM dynamics *in vivo*, and the quantitative metrics were defined to represent the pneumatic mobility and the middle ear pressure (MEP). The LCI measurements and the quantitative metrics were tested and validated with phantom models and a healthy adult volunteer. In order to further assess the clinical significance of the system in relation to OM, the pneumatic LCI datasets (traces of the TM position in response to the pressure stimulus, and the video otoscopic image of the TM) were acquired for 42 ears from 30 pediatric subjects. The TM displacement and pressure were measured, followed by tympanometry, and the two metrics (compliance and amplitude ratio) were computed to quantify the TM mobility and to estimate MEP.

5.2 PHANTOM STUDIES

The pneumatic LCI measurements were first collected from the middle ear phantom with different input pressure stimuli, and with different amount and types of simulated MEEs. According to **Equation (9)**, the displacements of the simulated TM measured by the pneumatic LCI system were converted into the compliance for further analysis.

5.2.1 Effect of Input Pressure Parameters on Phantom

The first phantom experiment focused on determining if the pneumatic compliance was independent of the parameters of the pressure transients (intensity and frequency), but dependent on middle ear conditions. Three phantom groups (simulated normal, fully filled simulated serous MEEs (water), and simulated thicker TM group with two thin films) were measured by the

pneumatic LCI system with pressure intensities of 5 to 50 mmHg, and the compliances are plotted in **Figure 18**. Each group showed a unique range of the compliance, regardless of the varied pressure intensities, suggesting that the compliance is independent of the intensity of the pressure, if within 5 to 50 mmHg. Most measurements were performed at 10 to 15 mmHg, as this range provided gentle but sufficiently strong pressure, and was used later for clinical studies.

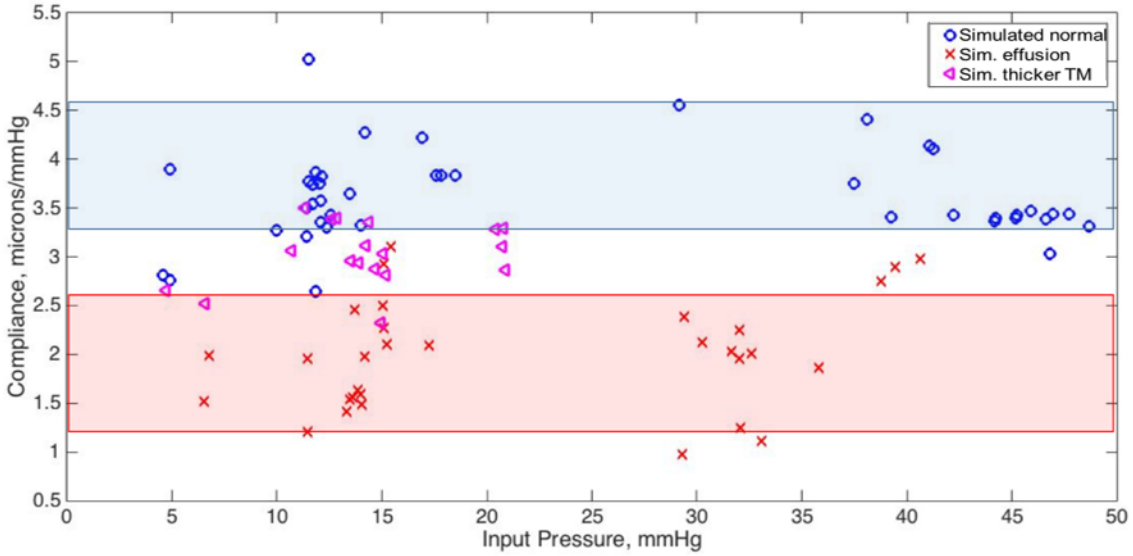

***Figure 18**. Compliance measured with different intensities of input pressure transients. Blue and red shaded regions include roughly 80% of measurements in the simulated normal and effusion group, respectively. Stronger input pressure intensities (greater than 25 mmHg) were only performed with the simulated normal and effusion groups.*

Similarly, the compliances after applying a range of frequencies (1 to 50 Hz) with constant maximum intensity of 12 mmHg of pressure transients were represented in **Figure 19**. Most measurements were performed with a frequency of less than 15 Hz, as the pressure module typically generates pressure stimuli within 10 Hz. It was observed that the datasets were separated based on the characteristics of the group, independent of the frequency of the pressure transients applied to the ear model. Note that besides three simulated normal phantom group, the measurements from a healthy volunteer were also included. The compliance measured from the

healthy volunteer was within the range of the compliances measured from the simulated normal phantom group.

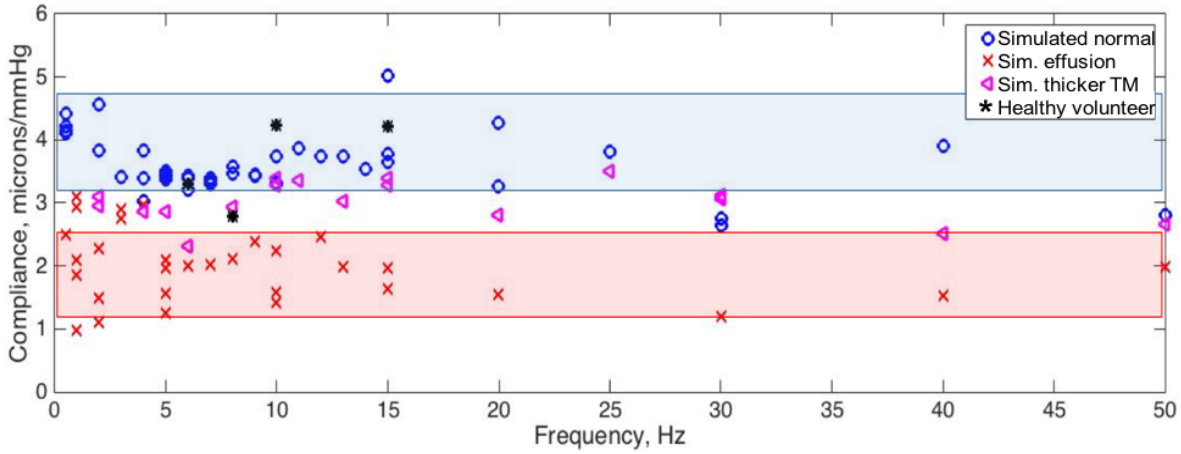

Figure 19. *Compliance measured with different frequencies of input pressure transients. Blue and red shaded region include roughly 80% of measurements in the simulated normal and effusion group, respectively. In addition to three phantom groups, four measurements from a healthy adult volunteer are included for comparison.*

5.2.2 Effect of Amount and Types of MEEs on Phantom

The previous phantom experiments showed that the measured compliances largely depended on different middle ear conditions, not input pressure parameters. The next phantom experiment studied the effect of MEEs in the middle ear cavity model on the compliance, with five different middle ear conditions (simulated normal, partially filled serous and mucoid MEEs, and fully filled serous and mucoid MEEs). As a result, the pneumatic compliance was significantly higher in the simulated normal than the simulated MEE group, as expected ($p<0.001$, **Table 2**). Note that the compliance depends on the amount of fluid that filled the middle ear cavity, or in other words, the volume of air present in the middle ear cavity. Only the compliances between fully filled simulated serous and mucoid MEEs showed no statistical difference, and this can be explained that the added mass from fully filled fluid would greatly inhibit the mobility of the TM, regardless of the viscosity

of the fluid. The above findings that the compliance depends on the presence of fluid and the volume of air in the middle ear cavity are supported from past studies, but the effect of different viscosities on the TM mobility has remained controversial, as some studies suggest that the effect of MEE viscosity on the decreased TM mobility is not as significant as the amount of fluid in the MEE [75-77]. This uncertainty may be partially due to the limitations of the measurement methods to determine if the loss of TM mobility depends on the presence, the amount, or the viscosity of MEEs, or any combinations of the above.

***Table 2**. Summarized result of the phantom experiment on different amount and viscosity of effusions.*

Group	Characteristic	Method	Compliance (μm/mmHg)	p-value with			
				Group 2	Group 3	Group 4	Group 5
1	Normal	One 20 μm plastic film	6.76 ± 1.24	<0.001	<0.001	<0.001	<0.001
2	Partially filled serous effusion	Plastic film with 1/4 filled water	5.11 ± 0.68	-	<0.001	<0.001	<0.001
3	Partially filled mucoid effusion	Plastic film with 1/4 filled petroleum jelly	3.41 ± 0.83		-	<0.001	<0.001
4	Full serous effusion	Plastic film with water	1.71 ± 0.45			-	**0.46**
5	Full mucoid effusion	Plastic film with petroleum jelly and water	1.55 ± 0.45				-

5.3 CLINICAL STUDIES

From the phantom studies, it was observed that the simulated MEEs in the middle ear cavity decreased the compliance measured by the pneumatic LCI system, and the compliance measurements were determined to be independent of the input intensity and frequency of the pressure transients if within 5-50 mmHg and 1-50 Hz. These ranges include the pressure stimuli parameters of the pneumatic LCI system used for human subjects. In this section, an *in vivo* experiment with a healthy adult volunteer was first performed to examine the spatially-varying TM mobility. This is followed by a clinical study with pediatric subjects to assess the changes in the TM dynamics during OM.

5.3.1 Human Subject Testing

Examining if the measurements and the metrics are dependent on the spatial position on the human TM was important to understand the spatially-varying TM dynamics. Pneumatic LCI measurements were performed on four TM quadrants (anterior inferior – AI, anterior superior – AS, posterior superior – PS, and posterior inferior – PI), and the measured compliance from each position on the TM are shown in **Figure 20**. A total of 15 measurements (on AI – 5, AS – 4, PS – 3, and PI – 3) were performed by the pneumatic LCI system. As a result, the measurements taken within the anterior areas (AI and AS) were not statistically different ($p=0.07$), and those taken within the posterior areas (PS and PI) were not significantly different ($p=0.20$) as well. However, the measurements taken from the anterior regions were statistically different ($p<0.001$) from those taken from the posterior regions. Thus, to maintain the consistency between measurements, the measurements were taken near the light reflex area on the TM (in AI) for the clinical studies if possible.

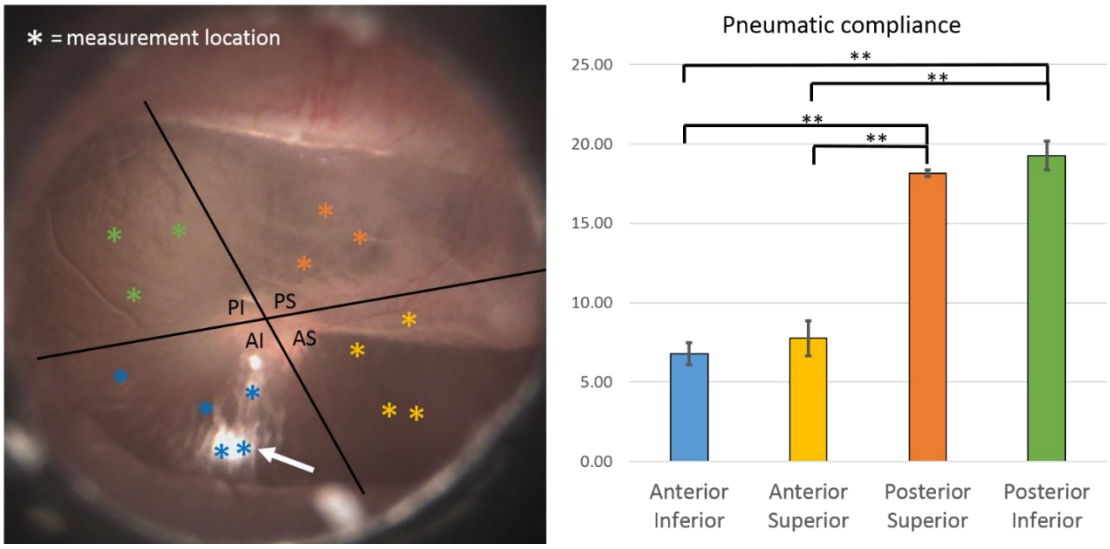

***Figure 20**. Compliance measured from different spatial positions on the TM of a healthy adult volunteer. Left figure shows an otoscopic view of the TM, and the bar graph on right illustrates statistics of the measurements. The error bars were calculated from all measurements in each quadrant, and each measurement is denoted as an asterisk in the left figure. White arrow on left figure indicates the cone of light. In the bar chart, ** denotes statistically significant difference ($p<0.001$) by the Student's t-test.*

5.3.2 Pneumatic LCI Measurements on Pediatric Subjects

A summary of the datasets from pediatric subjects, including pneumatic LCI, tympanometry, and physician diagnosis, is shown in **Table 3**. The pneumatic-induced displacement and dynamics of the TM in normal ears and ears with MEE are described herein. Representative pneumatic LCI datasets from a normal subject (subject A5) are shown in **Figure 21(A).** Note that the pneumatic LCI system also provided the surface view of the TM at the same time as the depth information (M-mode) and the pressure measurements were performed. Background room noise was kept to a minimum, and was found to not interfere significantly with the relatively large pneumatic-induced motion of the TM, occurring on the tens-of-microns scale. This subject visited the clinic for a non-ear related issue, and the normal ear condition was confirmed by the physician. For the cases with normal subjects, the TM displacements overlaid with the pressure measurements (**Figure 21(C)**) showed that the dynamics of the TM closely follow the pressure stimulus waveform.

As observed in **Figure 21(A),** the maximum displacement of the TM towards the middle ear cavity rapidly occurs as positive pressure is applied. Once the maximum positive pressure is reached, both the TM displacement and pressure start to gradually decrease due to the small leakage in the system and the partially sealed ear canal. A complete sealing of the ear canal is difficult to achieve, and less desirable because it would be uncomfortable. A partially sealed ear canal provides an inherent relaxation mechanism for the TM as the pressurized air is leaked out. A rapid decrease of the measured ear canal pressure would indicate a poorly sealed ear canal, which would subsequently require re-acquisition of the data.

As the pneumatic bulb returned to its original resting state, negative pressure (suction) was applied to the ear canal, creating a negative TM displacement (outward). Considering that a pneumatic bulb generates both positive and negative pressure with a similar intensity (roughly 150

daPa), it was surprising that the outward TM displacement was significantly greater (25% greater in this case) than the inward TM displacement. This suggests that the pressure difference between the ear canal and middle ear was less when the negative pressure was applied, indicating a negative MEP. This was confirmed with tympanometry (MEP of -20 daPa) and validated by the literature where it is noted that normal middle ears tend to have slightly negative MEP [33].

Table 3. A summary of datasets acquired from pediatric subjects.

			Pneumatic LCI	
Ear #	Diagnosis	Tympanogram	Compliance (μm/mmHg)	Amplitude Ratio
A1	Normal	A	7.08	2.09
A2	Normal	A	8.55	2.40
A3	Normal	A	5.92	2.40
A4	Normal	A	9.67	1.55
A5	Normal	A	7.52	2.69
A6	Normal	A	8.19	4.16
A7	Normal	A	5.38	5.42
A8	Normal	A	6.89	1.74
A9	Normal	A	11.30	2.94
A10	Normal	A	9.40	1.20
A11	Normal	A	10.70	1.14
A12	Normal	A	5.49	1.10
A13	Normal	A	5.49	1.10
A14	Normal	A	6.45	5.05
A15	Normal	A	5.40	2.65
A16	Normal	A	9.49	5.89
A17	Normal	A	6.34	2.39
A18	Normal	A	9.94	4.66
A19	Normal	A	9.32	1.85
A20	Normal	A	8.61	2.35
A21	Normal	A	5.18	1.54
A22	Normal	A	8.30	1.22
A23	Normal	A	3.34	3.45
A24	URI	A	4.16	2.33
A25	URI	A	6.92	3.72
A26	URI	A	5.20	3.30
A27	URI	A	8.72	4.15
A28	OME	A	3.43	1.31
B1	Normal	B	3.91	1.62
B2	URI	B	2.20	0.00
B3	OME	B	5.04	0.88
B4	AOM	B	6.29	0.25
B5	AOM	B	3.30	1.52
B6	AOM	B	2.36	0.95
B7	AOM	B	4.40	0.40
C1	Normal	C	2.00	0.75
C2	URI	C	3.38	4.20
C3	URI	C	6.80	4.80
C4	OME	C	1.69	2.48
C5	OME	C	1.94	2.03
C6	OME	C	4.30	0.90
C7	OME	C	1.13	0.81

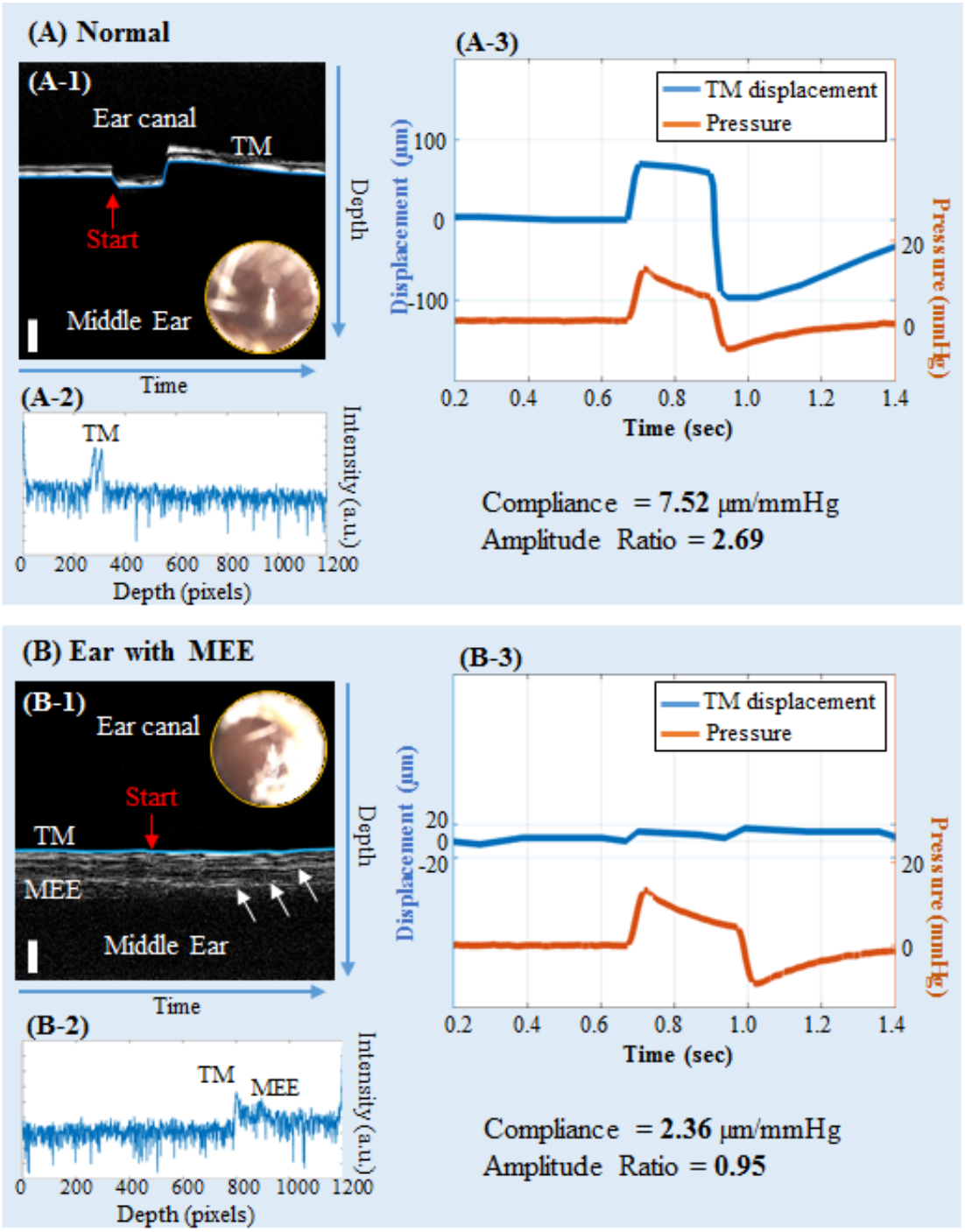

Figure 21. *Representative pneumatic LCI datasets from (A) normal pediatric subject and (B) pediatric subject with OM. (A-1) and (B-1) show M-scans of the TM when pressure was applied. The start of the pneumatic stimulus is indicated with a red arrow. The inset images in (A-1) and (B-1) show the corresponding en face surface views of the TM. (A-2) and (B-2) represent A-scans. (A-3) and (B-3) illustrate the plot of the TM displacement and the pressure dynamics. The compliance and amplitude ratio are calculated based on* ***Equation (9)*** *and* ***(10).*** *The scale bars represent 200 μm in depth. a.u.: arbitrary units.*

5.3.3 Pneumatic LCI Metrics Compared with Tympanometry

In addition to the pneumatic LCI measurements, standard tympanometry was performed on the pediatric subjects to determine if there is a relationship between pneumatic and acoustic mobility, although acoustic stimuli from tympanometry (~70 dB sound pressure level (SPL), which can be converted to roughly 0.63 daPa) induce nano-scale TM displacements, whereas pneumatic stimuli from the pneumatic LCI system (~150 daPa) cause micron-scale TM displacements. Furthermore, the comparison with the MEP determined by tympanometry validated the capability of the amplitude ratio in estimating the MEP.

Firstly, the compliance (pneumatic mobility) measured from pneumatic LCI and peak admittance (PA) (acoustic mobility) were compared, regardless of the pathological conditions. **Figure 22(A)** indicates that the compliance and PA are slightly correlated (R^2 of 0.22), and in **Figure 22(B),** the amplitude ratio and MEP show a stronger linear relationship with an R^2 value of 0.53. The lower correlation between the compliance and the PA is expected because those indicate two distinct parameters; the compliance depends directly on the measured TM displacement, while the PA is a relative measure of the acoustic admittance in the middle ear. The relationship between the amplitude ratio and the MEP suggests that the higher amplitude ratio corresponds to a more negative MEP. The amplitude ratio close to or less than 1 may indicate positive MEP. The MEPs of ears with 'Type B' tympanograms were estimated to be positive (average of 35 daPa), which cannot be determined otherwise. The positive MEP was likely from the accumulation of fluid and pressure associated with the MEE.

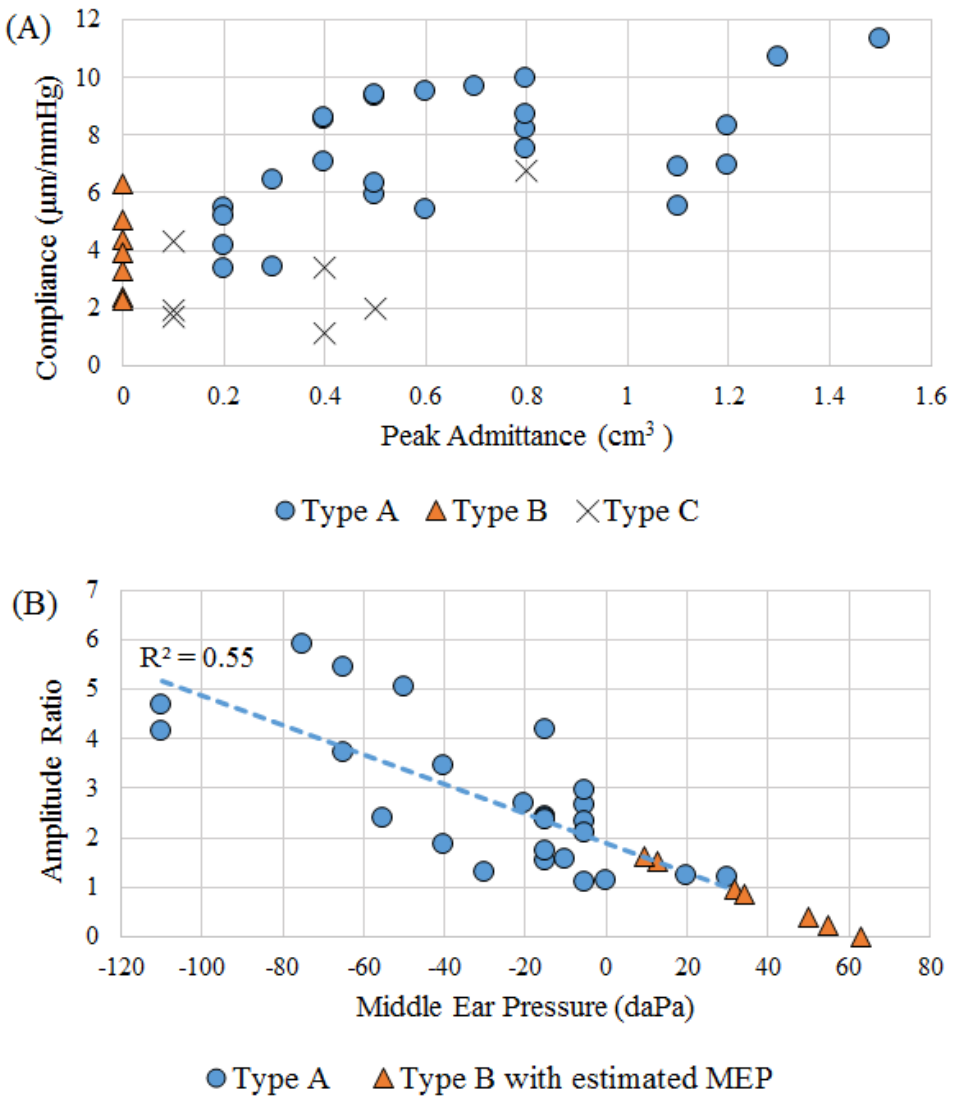

Figure 22. *Pneumatic LCI measurements compared with tympanometry. (A) Comparison of the compliance (pneumatic mobility) from pneumatic LCI and the peak admittance (acoustic mobility) from tympanometry. (B) A linear relationship (a linear coefficient R^2) between the amplitude ratio and the MEP from tympanometry, suggesting that the amplitude ratio may be an indicative of the MEP. The MEPs of ears with a 'Type B' tympanogram were estimated based on the amplitude ratio.*

Next, the subjects were categorized based on tympanogram types ('A', 'B', and 'C') and physician diagnosis ('normal', 'MEE', and 'URI') to further assess the clinical relevance of the quantitative metrics, and to closely examine each dataset. In **Figure 23**, ears with 'Type A' tympanograms and the normal ear group can be roughly separated from ears with 'Type B'

tympanograms and the MEE group based on the pneumatic LCI metrics, with the exception of the subject A28 (diagnosed with OM with effusion, but found to have a 'Type A' tympanogram). This subject likely had a small MEE without severe TM inflammation, causing a smaller decrease in acoustic TM mobility. This case also exemplifies a limitation of tympanometry with its low negative predictive value. Overall, the MEE group tended to have both lower compliance and a lower amplitude ratio, as expected. There was no specific trend for ears with 'Type C' tympanograms or the URI group. However, based on the pneumatic LCI metrics, it can be expected that the data points within the blue oval shape in **Figure 23** do not contain a MEE, whereas the data points within the red oval shape have a MEE. This assumption correlated well with physician diagnosis, demonstrating the clinical potential of these pneumatic LCI metrics. The pneumatic mobility, measured by pneumatic LCI, may be more sensitive at detecting the early stages of MEE accumulation due to the high spatial and temporal resolution of LCI.

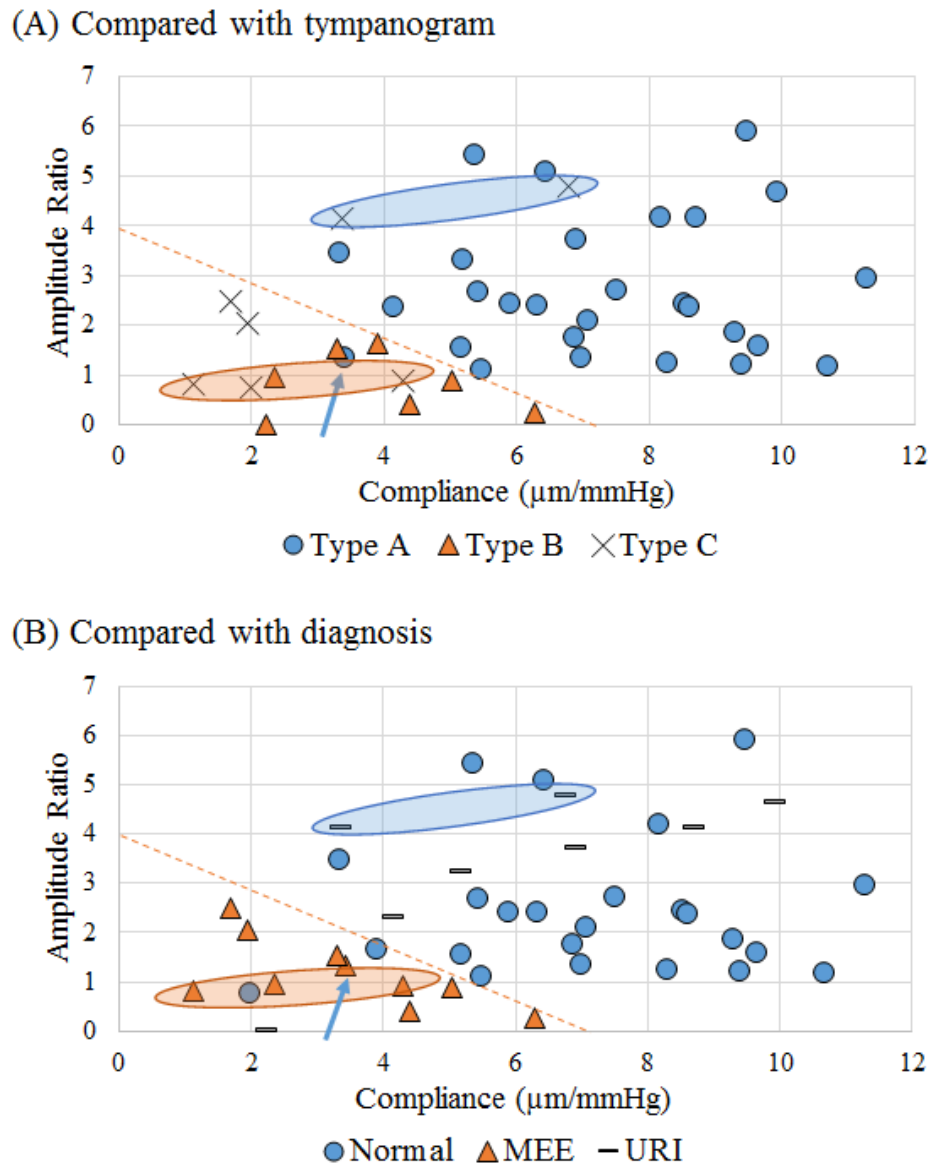

***Figure 23**. The entire 42 datasets plotted based on the quantitative metrics, compliance and amplitude ratio.*

Although the two quantitative metrics were able to separate the datasets with different pathological conditions, statistical analysis was necessary to underline the capability of the metrics. In **Figure 24(A)**, the statistical analysis validates that both the compliance and amplitude ratio are significantly less in the cases of MEE and 'Type B' tympanogram than the normal and 'Type A' tympanograms ($p<0.001$). The compliance of 'Type A' is also greater than that of 'Type

C' ($p<0.001$), agreeing with tympanometry that 'Type A' possesses greater acoustic compliance. However, the amplitude ratios of 'Type A' and 'Type C' were not statistically different ($p>0.05$). This is because the amplitude ratio may not have enough sensitivity to determine a strong negative MEP due to the limited strength of the pressure sweep. The statistical difference in the amplitude ratio of 'Type B' and 'Type C' ($p<0.05$) is not surprising, as the MEP of 'Type B' is generally positive, while that of 'Type C' is negative. The compliance of 'Type B' versus 'Type C' was not significantly different ($p>0.05$), although both types showed statistically less compliance when compared with 'Type A' ($p<0.001$). It is meaningful to note that 'Type B' showed no acoustic mobility, but its pneumatic TM mobility was comparable to that of 'Type C'. This is because the strong pressure conditions of both 'Type B' and 'Type C' yield less compliance. The statistical comparison suggests that the metrics of pneumatic LCI highly agree with the parameters of tympanometry.

Figure 24(B) draws similar comparisons as **Figure 24(A),** but based on the physician diagnosis. Both the compliance and amplitude ratio of the MEE group were significantly less than that of the normal group ($p<0.001$ and $p<0.01$, respectively). These greater p-values of the analysis with physician diagnosis compared to that of the tympanogram imply that the pneumatic LCI metrics are more comparable with the tympanometric measurements than with the physician diagnosis. This was anticipated, because tympanometry provides quantitative measurements for similar metrics as in pneumatic LCI (mobility and MEP), while a physician's diagnosis is made based on multiple qualitative factors such as patient history, physical symptoms, and the observed visual features of the TM.

In **Figure 24(B),** the normal group showed a significantly greater ($p<0.05$) compliance than the URI group. This again agrees with tympanometry and suggests that the normal TM

contains greater pneumatic as well as acoustic compliance. The amplitude ratio of the URI group was the largest, indicating that the URI group has the strongest negative MEP. When compared with the MEE group, the amplitude ratio of the URI group was significantly greater ($p<0.01$) because the MEE group has a positive MEP. The tables embedded in **Figure 24** summarize these statistical findings.

(A) Compared with tympanogram

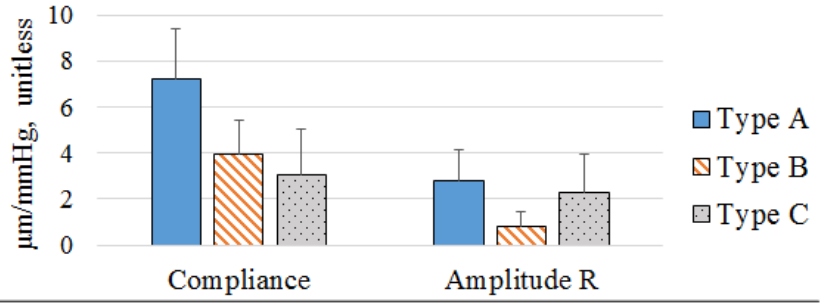

	Type A	Type B	Type C	*p*-value between A-B	*p*-value between A-C	*p*-value between B-C
Compliance (μm/mmHg)	7.2 ± 2.2	3.9 ± 1.5	3.0 ± 1.9	**<0.001**	**<0.001**	0.35
Amplitude R	2.8 ± 1.4	0.8 ± 0.6	2.3 ± 1.6	**<0.001**	0.42	**<0.05**

(B) Compared with diagnosis

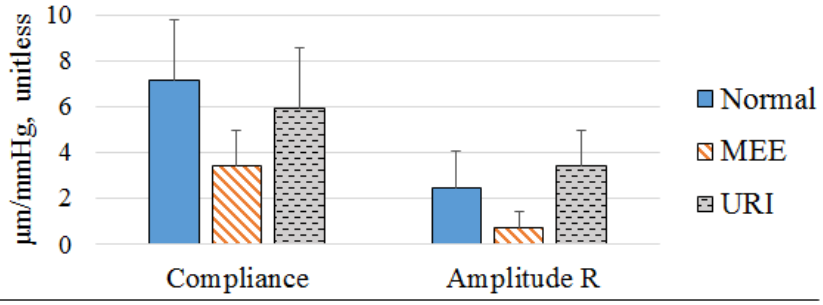

	Normal	MEE	URI	*p*-value between Normal-MEE	*p*-value between Normal-URI	*p*-value between MEE-URI
Compliance (μm/mmHg)	7.1 ± 2.3	3.4 ± 1.6	5.9 ± 2.6	**<0.001**	**<0.05**	0.14
Amplitude R	2.5 ± 1.4	0.7 ± 0.7	3.4 ± 1.6	**<0.01**	0.40	**<0.01**

Figure 24. *Statistical analysis of the quantitative metrics defined by the pneumatic LCI system. (A) Comparion based on tympanogram types. (B) Comparison based on physician diagnosis.*

6 DISCUSSION

6.1 OVERVIEW

While pneumatic otoscopy allows physicians to observe visual characteristics and the general motion of the TM in response to an applied pressure change, small changes in the mobility of the TM can be extremely difficult to visually detect. This study demonstrates that pneumatic LCI otoscopy can provide quantitative measurements of the TM dynamics with micron-scale resolution, while maintaining the visual benefits of pneumatic otoscopy. Pneumatic LCI provides a set of multidimensional data: TM displacement, pressure measurement, an *en face* color view of the TM, and depth-resolved measurements into the middle ear cavity. Utilizing a pneumatic bulb in the pressure module allows the induction of a pressure transient with both negative and positive pressure, so that physicians can examine both the retracted and bulging TM, just like standard pneumatic otoscopy. The objective and quantitative metrics (compliance and amplitude ratio) are defined to represent the pneumatic mobility of the TM and the MEP, comparable to tympanometric measurements. In this section, these quantitative metrics are further explained in relation to the pathophysiology of OM, and comparisons with other middle ear diagnostic tools are made and discussed.

6.2 CLINICAL SIGNIFICANCE OF PNEUMATIC LCI OTOSCOPY

Pneumatic LCI otoscopy is a unique and valuable method to examine middle ear dynamics, as it can generate both anatomical and functional information about the middle ear. Furthermore, the structural information from both an RGB surface view of the TM and the depth-resolved LCI information may increase the accuracy in determining a presence of a MEE, a key determinant to establish the diagnosis of OM. In this section, more explanation in understanding the pneumatic

LCI metrics and the effect of pneumatic stimuli are included. The clinical significance of the pneumatic LCI system is discussed with a comparison of current middle ear diagnostic methods.

6.2.1 Quantitative Metrics of Pneumatic LCI

It has been known that the presence of a middle ear effusion (MEE) decreases both acoustic and pneumatic mobility of the TM due to the added mass and viscosity from the MEE [32, 78]. Thus, quantifying the TM displacement has been of great interest to understand TM mobility loss caused by the presence of MEE and altered MEP. By capturing the pneumatic-induced motion of the TM, the pneumatic LCI system may offer new parameters to study TM dynamics in OM. The compliance calculates the TM displacement per unit pressure, and was also introduced and discussed in our previous study [57]. This metric converts the TM mobility examined from standard pneumatic otoscopy to an objective parameter. As expected, a MEE significantly reduced the TM compliance, agreeing with our previous study on adult subjects. Nonetheless, low compliance itself was not sufficient to determine the presence of a MEE. However, the depth-resolved imaging capability of LCI offers the ability to detect optically scattering particles that may exist within a MEE, and thereby provide a clear diagnostic marker for a MEE.

Besides mobility, pneumatic otoscopy can also be used to examine the position of the TM (retracted or bulging), which augments the qualitative assessment of MEP. The amplitude ratio converts this position of the TM to the quantitative MEP, based on the comparison of the TM displacements in two opposite directions. This comparison has already been performed by physicians using pneumatic otoscopy, but accurate comparison is difficult due to the on-axis motion of the TM. LCI may be the most suitable imaging modality to measure this on-axis motion of the TM, as it delivers depth-resolved information along the axial line of sight with high micron-

scale resolution. With simultaneous pressure measurements, the amplitude ratio can define the MEP, and may indicate the stage of the MEE and the degree of fluid accumulation. For example, subjects with MEEs and with the greater amplitude ratio (negative MEP) tend to be in the early-stage or recovering stage of OM, while most subjects with an amplitude ratio close to 0 (positive MEP) were diagnosed as having a full mucoid effusion.

Nonetheless, more pathological datasets are required to explore the capabilities of the pneumatic LCI metrics in differentiating middle ear conditions. Future studies will investigate the effect of the types and amount of MEE on the TM mobility by comparing the pneumatic LCI metrics with the cross-sectional OCT images of the middle ear, and will continue to build the normative database for different infection states using pneumatic LCI and pneumatic OCT otoscopy.

6.2.2 Effect of Input Pneumatic Stimuli

Analyzing the effect of pressure stimuli parameters (intensity and frequency) on the pneumatic LCI measurements was important to ensure that the quantitative metrics were independent of the input parameters, but dependent on the condition of the middle ear. As a linear relationship between the TM displacement and the pressure intensity was previously determined within the range of pressure intensities employed in the pneumatic LCI system [57], the compliance is independent of the intensity of the pressure stimuli. In addition, the minimal effect of pressure stimuli frequency on the measurements was investigated in the phantom and human volunteer studies, as shown in **Figure 19**.

On the other hand, the intensity of the pressure transients determines the MEP range that can be estimated by the pneumatic LCI system. If stronger pressure transients are employed,

subjects with greater MEP can be estimated from the amplitude ratio, although this may increase patient discomfort. However, since the pressure module of the pneumatic LCI system can easily adjust the pressure intensity, one can accordingly change the pressure intensity for the subjects suspected to have OM with effusion (OME) or an upper respiratory infections (URI), who typically present with larger negative MEPs [6].

6.2.3 Pneumatic LCI Compared with Other Diagnostic Methods

Although this study utilized tympanometry as a comparative diagnostic tool for pneumatic LCI, the main difference is that the prior estimates the acoustic mobility based on the amount of a reflected frequency tone from the TM, whereas the latter measures pneumatic (non-acoustic) mobility in response to the pressure transients. Thus, a direct comparison between those two techniques may not necessarily be appropriate. Nevertheless, the strengths of pneumatic LCI compared to tympanometry are discussed, as tympanometry is widely used by physicians and audiologists to examine the functioning of the middle ear. Pneumatic LCI provides TM compliance in response to pressure stimuli, and no other techniques can directly measure the depth-resolved mobility of the human TM *in vivo.* Pneumatic LCI can provide quantitative measurements regardless of the presence of a MEE, whereas tympanometry cannot for a 'Type B' tympanogram. The LCI measurements are less affected by a blockage of the ear canal than tympanometry, as pneumatic LCI employs a point-based depth-resolved measurement. Our system generates both an *en face* view of the TM surface as well as depth-resolved information, while tympanometry cannot deliver any visual information to the physicians, thus also requiring otoscopy. Furthermore, the depth-resolved information may directly and visually indicate the presence of a MEE (**Figure 21(B-2)**).

When compared to pneumatic otoscopy, pneumatic LCI offers automated and computer-controlled pressure transients from a pneumatic bulb, reducing the variability of the pressure pulses (intensity and durations) between physicians. The strength of the pressure transient is adjustable, and can be as low as 50 daPa because even subtle motions (tens of microns) of the TM can be measured by the system. These subtle motions are not readily visualized with the human eye, and therefore pneumatic LCI enables a more sensitive examination of TM mobility *in vivo*. Furthermore, the quantitative comparison between TM displacements in two opposite directions estimates MEP. The simultaneous pressure measurement can be used to notify users if there is any air leak during measurements. Overall, pneumatic LCI otoscopy can offer more dynamic information for subjects with MEE than tympanometry, and directly measure TM displacements with potentially gentler and more precisely controlled air pressure transients than pneumatic otoscopy.

6.3 LIMITATIONS

There are two major limitations of this thesis research. The first is the lack of a gold-standard for confirming a presence of a MEE due to the required invasive procedure of tympanocentesis, which involves a surgical incision of the TM and aspiration of the MEE. Given the relatively small sample volume of a MEE, particularly in pathological conditions, this collection and validation is extremely challenging and impractical in routine clinical exams.

While there are many advantages of pneumatic LCI as a quantitative middle ear diagnostic tool, there are also several challenges and limitations. The light ranging technique generates high-resolution depth-resolved information when the light is focused on or near the TM, and our handheld probe is specifically designed based on a standard ear speculum to help users guide the

light beam and selectively measure from the regions of interest. A single point-based measurement certainly cannot represent the overall TM mobility; however, all measurements were taken near the light reflex region of the TM, guided by the *en face* view of the TM during imaging. By positioning the LCI light beam over other regions of the TM, it is possible to assess subtle regional differences in TM mobility that may exist [57]. Another intrinsic challenge of any pneumatic device is the accuracy of the pressure measurement, which depends on the complete sealing of the speculum in the ear canal. A standard ear speculum with a rubber-made earbud provided a more secure and comfortable sealing of the ear canal compared to the traditional pneumatic ear specula. In addition, the seal of the ear canal can be readily checked from the pressure measurement of pneumatic LCI, which instills confidence in the measurement. The overall cost (roughly $ 50k) of this system is another factor since pneumatic LCI requires more expensive optical components, such as a low-coherence light source, detector, and optical fibers. We have reduced the cost of this system by removing the lateral scanning mechanism of OCT to create the LCI system that is based on point measurements. Moreover, a recent study from our group has focused on developing low-cost light ranging systems, increasing the potential of LCI as a readily available technique for primary care offices [79].

Despite these limitations, a significant advantage of pneumatic LCI otoscopy is that the entire time-dependent traces of the TM motions and the pressure stimulus are quantitatively recorded. Although only two metrics are defined for this study, more analysis and comparisons are possible, depending on the focus of the study.

7 CONCLUSION AND FUTURE DIRECTIONS

Although pneumatic otoscopy is highly recommended in care and treatment guidelines to assess TM mobility and determine the presence or absence of a MEE when diagnosing OM, its subjective information has challenged the proper application and interpretation of this technique. Pneumatic LCI otoscopy enables not only the surface visualization of the TM, but also the quantitative measurement of pneumatic-induced TM mobility, MEP, and the depth-resolved structural information in the middle ear cavity. The measurements acquired in this study showed that the pneumatic LCI metrics (compliance and the amplitude ratio) were significantly less in subjects with MEE, and the amplitude ratio can indicate the MEP. These findings suggest that pneumatic LCI can be used to determine the presence of MEE and quantify TM dynamics in subjects with MEE, as well as in normal subjects, with the combined benefits of standard otoscopy, pneumatic otoscopy, and tympanometry.

Future studies will continue to investigate the temporal dynamics and aspects of the TM motion in relation to the type and amount of MEE, determined next by high-speed cross-sectional OCT imaging. Follow-on studies will also compare the depth-resolved structures identified by OCT with middle ear power analysis [80], another middle ear diagnostic tool mainly used by audiologists, to observe the effect of changes in the middle ear structures on the acoustic measurements.

Lastly, optical, mechanical, and biological analysis of aspirated MEEs from human subjects will be performed to relate optical findings from OCT to our biological understanding. More specifically, the viscosity, scattering, and turbidity of MEEs will be analyzed and compared with bacterial load, cell counts, and physician diagnosis. This investigation will further enhance the capability of OCT to non-invasively examine both structural and functional information in the

middle ear dynamics directly relevant to OM pathophysiology, which will help physicians more accurately diagnose and monitor OM.

8 REFERENCES

1. Marvin, K., A. Ambrosio, and M. Brigger, *The increasing cost of pediatric otolarynglogy care*, in *2017 Annual Meeting for American Academy of Otolaryngology - Head and Neck Surgery Foundation*. 2017: Chicago, IL.
2. Rosa-Olivares, J., et al., *Otitis media: to treat, to refer, to do nothing: a review for the practitioner.* Pediatrics in Review, 2015. **36**(II): p. 480-488.
3. *What is an otoscope - history and use*. 2014 [cited 2017 October 30th]; Available from: http://www.baronmedical.com/blog/what-is-an-otoscope/.
4. Lieberthal, A.S., et al., *The diagnosis and management of acute otitis media.* Pediatrics, 2013. **131**(3): p. e964-999.
5. Casey, J.R. and M.E. Pichichero. *Acute otitis media: Update 2015*. 2015 [cited 2017 July 24]; Available from: http://contemporarypediatrics.modernmedicine.com/contemporary-pediatrics/news/acute-otitis-media-update-2015.
6. Rosenfeld, R.M., et al., *Clinical practice guidelines: otitis media with effusion (update).* Otolaryngol Head Neck Surg. , 2016. **154**(1S): p. S1-S41.
7. Takata, G.S., et al., *Evidence Assessment of the Accuracy of Methods of Diagnosing Middle Ear Effusion in Children With Otitis Media With Effusion.* Pediatrics, 2003. **112**(6): p. 1379-1387.
8. Abbott, P., et al., *The effect and acceptability of tympanometry and pneumatic otoscopy in general practitioner diagnosis and management of childhood ear disease.* BMC Family Practice, 2014. **15**: p. 181.
9. Jones, W.S. and P.H. Kaleida, *How helpful is pneumatic otoscopy in improving diagnostic accuracy?* Pediatrics, 2003. **112**: p. 510-513.
10. Pichichero, M.E., *Otitis media.* Pediatr Clin N Am, 2013. **60**: p. 391-407.
11. Teele, D.W., et al., *Epidemiology of otitis media during the first seven years of life in children in greater Boston: a prospective, cohort study.* J Infect Dis. , 1989. **160**: p. 83-94.
12. Vergison, A., et al., *Otitis media and its consequences: beyond the earache.* Lancet Infect Dis. , 2010. **10**: p. 195-203.
13. Monasta, L., et al., *Burden of disease caused by otitis media: systematic review and global estimates.* PLoS ONE, 2012. **7**(4): p. e36226.
14. van den Aardweg, M.T., et al., *Adenoidectomy for otitis media in children [review]*. Cochrane Database Syst Rev., 2010. **1**: p. CD007810.
15. Coticchia, J.M., et al., *New paradigms in the pathogenesis of otitis media in children.* Frontiers in Pediatrics, 2013. **1**(52): p. 1-7.
16. ByHealthwise, *Ear anatomy*. 2015, WebMD.
17. DiMaio, F.H.P. and J. Tonndorf, *The terminal zone of the external auditory meatus in a variety of mammals.* Arch Otolaryngol, 1978. **104**: p. 570-575.
18. Ravicz, M.E., J.T. Cheng, and J.J. Rosowski, *Sound pressure distribution within natural and artificial human ear canals: forward stimulation.* The Journal of the Acoustical Society of America, 2014. **136**: p. 3132.
19. Cheng, J.T., et al., *The effect of ear canal orientation on tympanic membrane motion and the sound field near the tympanic membrane.* J Assoc Res Otolaryngol., 2015. **16**: p. 413-432.
20. Mosby, I., an affiliate of Elsevier Inc., *Quadrants of eardrum*. 2007.

21. Lim, D.J., *Functional morphology of the mucosa of the middle ear and Eustachian tube.* Annals of Otology, Rhinology & Laryngology, 1976. **85**(2_suppl): p. 36-43.
22. Murphy, T.F., T. Chonmaitree, and S. Barenkamp, *Microbiology and immunology panel.* Otolaryngol Head Neck Surg., 2013. **148**(Suppl 4): p. E64-E89.
23. Coker, T.R., et al., *Diagnosis, microbial epidemiology, and antibiotic treatment of acute otitis media in children.* Journal of the American Medical Association 2010. **304**(19): p. 2161-2169.
24. Bluestone, C.D. and J.O. Klein, *Otitis media in infants and children*. 2007: PMPH-USA.
25. ENTclinic, *The Eustachian Tube*. 2012.
26. Chris, O., *Ear infections and fluid in the middle ear can cause speech delays*. 2013.
27. Paradise, J.L., et al., *Tympanostomy tubes and developmental outcomes at 9 to 11 years of age.* N Engl J Med, 2007. **356**: p. 248-261.
28. Osma, U., S. Cureoglu, and S. Hosoglu, *The complications of chronic otitis media: report of 93 cases.* The Journal of Laryngology and Otology, 2000. **114**: p. 97-100.
29. Pichichero, M.E. and M.D. Poole, *Assesing diagnostic accuracy and tympanocentesis skilss in the management of otitis media.* Arch Pediatr Adoles Med., 2001. **155**: p. 1137-1142.
30. WelchAllyn, *MacroView Otoscope*, M. Otoscope, Editor. 2017, www.welchallyn.com.
31. Blomgren, K. and A. Pitkaranta, *Is it possible to diagnose acute otitis media accurately in primary health care?* Family Practice, 2003. **20**(5): p. 524-527.
32. Cavanaugh, R.M., *Pediatricians and the pneumatic otoscope: are we playing it by ear?* Pediatrics, 1989. **84**(2): p. 362-364.
33. Onusko, E., *Tympanometry.* Am Fam Physician., 2004. **70**(9): p. 1713-1720.
34. WelchAllyn, *TM 286 Autotymp Tympanometric System.* 2017.
35. FirstYears. *Tympanometry*. 2003; Available from: http://www.firstyears.org/tests/tymph.htm.
36. Palmu, A.A., et al., *Diagnostic value of tympanometry in infants in clinical practice.* Int J Pediatr Otorhinolaryngol., 1999. **49**: p. 207-213.
37. Anwar, K., et al., *Otitis media with effusion: Accuracy of tympanometry in detecting fluid in the middle ears of children at myringotomies.* Pak J Med Sci., 2016. **32**(2): p. 466-470.
38. Voss, S.E. and J.B. Allen, *Measurement of acoustic impedance and reflectance in the human ear canal.* J Acoust Soc Am., 1994. **95**: p. 372-384.
39. Keefe, D.H., et al., *Ear-canal impedance and reflection coefficient in humn infants and adults.* J Acoust Soc Am., 1993. **94**(5): p. 2617-2638.
40. Voss, S.E., G.R. Merchant, and N.J. Horton, *Effects of middle-ear disorders on power reflectance measured in cadaveric ear canals.* Ear Hear, 2012. **33**(2): p. 195-208.
41. Hunter, L.L., et al., *Pediatric applications of wideband acoustic immitance measures.* Ear Hear, 2013. **34**: p. 36s-42s.
42. Keefe, D.H. and J.L. Simmons, *Energy transmittance predicts conductive hearing loss in older children and adults.* J Acoust Soc Am., 2003. **114**(6 Pt 1): p. 3217-3238.
43. Rosenfeld, R.M., *Diagnostic certainty for acute otitis media.* Int J Pediatr Otorhinolaryngol., 2002. **64**(2): p. 89-95.
44. Huang, D., et al., *Optical Coherence Tomography.* Science, 1991. **254**(5035): p. 1178-1181.
45. Monroy, G.L., et al., *Handheld optical coherence tomograpy: technologies and applications.* J Biomed Opt, 2017. **Under review**.

46. Zysk, A.M., et al., *Optical coherence tomography: a review of clinical development from bench to bedside.* J Biomed Opt, 2007. **12**(5): p. 051403.
47. Vakoc, B.J., et al., *Cancer imaging by optical coherence tomography: preclinical progress and clinical potential.* Nature Reviews Cancer, 2012. **12**(363-368).
48. Boppart, S.A. and R. Richards-Kortum, *Point-of-care and point-of-procedure optical imaging technologies for primary care and global health.* Science Translational Medicine, 2014. **6**(253rv2).
49. Jung, W., et al., *Handheld optical coherence tomography scanner for primary care diagnostics.* IEEE Transactions on Biomedical Engineering, 2011. **58**(3): p. 741-744.
50. Shelton, R.L., et al., *Optical coherence tomography for advanced screening in the primary care office.* J Biophotonics, 2014. **7**: p. 525-533.
51. Pitris, C., et al., *High-resolution imaging of the middle ear with optical coherence tomography.* Arch Otolaryngol Head Neck Surg, 2001. **127**: p. 637-642.
52. MacDougall, D., et al., *Optical coherence tomography system requirements for clinical diagnostic middle ear imaging.* J Biomed Opt, 2015. **20**(5): p. 056008.
53. Nguyen, C.T., et al., *Noninvasive optical interferometry for the assessment of biofilm growth in the middle ear.* Biomed Opt Express, 2010. **1**: p. 1104-1116.
54. Nguyen, C.T., et al., *Noninvasive in vivo optical detection of biofilm in the human middle ear.* Proc Natl Acad Sci., 2012. **109**: p. 9529-9534.
55. Monroy, G.L., et al., *Noninvasive depth-resolved optical measurements of the tympanic membrane and middle ear for differentiating otitis media.* Laryngoscope, 2015. **125**(8): p. E276-282.
56. Monroy, G.L., et al., *Non-invasive optical assessment of viscosity of middle ear effusions in otitis media.* J Biophotonics, 2016. **10**: p. 394-403.
57. Shelton, R.L., et al., *Quantitative Pneumatic Otoscopy Using a Light-Based Ranging Technique.* J Assoc Res Otolaryngol., 2017. **18**(4): p. 555-568.
58. Van der Jeught, S., et al., *Full-field thickness distribution of human tympanic membrane obtained with optical coherence tomography.* J Assoc Res Otolaryngol., 2013. **14**: p. 483-494.
59. Bakaletz, L.O., *Bacterial biofilms in otitis media.* The Pediatric Infectious Disease Journal, 2007. **26**(10): p. S17-S19.
60. Hubler, Z.M.L., et al., *Real-time automated thickness measurements of the in vivo human tympanic membrane using optical coherence tomography.* Quantitative Imaging in Medicine and Surgery, 2015. **5**: p. 69-77.
61. Pande, P., et al., *A Mosaicking approach for in vivo thickness mapping of the human tympanic membrane using low coherence interferometry.* J Assoc Res Otolaryngol., 2016.
62. Park, J., et al., *Investigation of middle ear anatomy and function with combined video otoscopy-phase sensitive OCT.* Biomed Opt Express, 2016. **7**(2): p. 240-250.
63. MacDougall, D., et al. *Clinical swept-source optical coherence tomography of the middle ear*. in *Biomedical Optics Congress*. 2016. OSA.
64. MacDougall, D., et al. *Real-time swept-source Doppler optical coherence tomography for middle ear diagnostics*. in *OSA*. 2015.
65. Bedard, N., et al., *Light field otoscope design for 3D in vivo imaging of the middle ear.* Biomed Opt Express, 2017. **8**(1): p. 260-272.
66. Carr, J.A., et al., *Using the shortwave infrared to image middle ear pathologies.* Proc Natl Acad Sci., 2016. **113**(36): p. 9989-9994.

67. Valdez, T.A., et al., *Multiwavelength fluorescence otoscope for video-rate chemical imaging of middle ear pathology.* Analytical Chemistry, 2014. **86**: p. 10454-10460.
68. Flores-Moreno, J.M., et al., *Holographic otoscope for na-displacement measurements of surfaces under dynamic excitation.* Scanning, 2011. **33**(5): p. 342-352.
69. Ng, R., et al., *Light field photography with a hand-held plenoptic camera.* Computer Science Technical Report CSTR, 2005. **2**(11): p. 1-11.
70. Varrasso, D.A., *Otitis media: the need for a new paradigm in medical education.* Pediatrics, 2006. **118**: p. 1731.
71. Jaisinghani, V.J., et al., *Quantitative analysis of tympanic membrane disease using video-otoscopy.* Laryngoscope, 2000. **110**(10): p. 1726-1730.
72. Cho, Y.-S., et al., *Video pneumatic otoscopy for the diagnosis of otitis media with effusion: a quantitative approach.* Eur Arch Otorhinolaryngol., 2009. **266**(7): p. 967-973.
73. Takeuchi, K., et al., *Viscoelastic properties of middle ear effusions from pediatric otitis media with effusion and their relation to gross appearance.* Eur Arch Otorhinolaryngol., 1990. **247**: p. 60-62.
74. Fay, J.P., S. Puria, and C.R. Steele, *The discordant eardrum.* Proc Natl Acad Sci., 2006. **103**(52): p. 19743-19748.
75. Dai, C., M.W. Wood, and R.Z. Gan, *Combined effect of fluid and pressure on middle ear functions.* Hear Res., 2008. **236**(1-2): p. 22-32.
76. Guan, X. and R.Z. Gan, *Mechanisms of tympanic membrane and incus mobility loss in acute otitis media.* J Assoc Res Otolaryngol., 2013. **14**(3): p. 295-307.
77. Guan, X., Y. Chen, and R.Z. Gan, *Factors affecting loss of tympanic membrane mobility in acute otitis media model of chinchilla.* Hear Res., 2014. **309**: p. 136-146.
78. Allen, J.B., P.S. Jeng, and H. Levitt, *Evaluation of human middle ear function via an acoustic power assessment.* J Rehabil Res Dev, 2005. **42**: p. 63-78.
79. Pande, P., et al., *Low-cost hand-held probe for depth-resolved low coherence interferometry.* Biomed Opt Express, 2017. **8**(1): p. 338-348.
80. Nguyen, C.T., et al., *Investigation of bacterial biofilm in the human middle ear using optical coherence tomography and acoustic measurements.* Hear Res., 2013. **301**: p. 193-200.